Applied Water Science (2024) 14:209
https://doi.org/10.1007/s13201-024-02238-8

ORIGINAL ARTICLE

Removal of antibiotics from aqueous solutions: insights of competitive adsorption onto Ni-impregnated biochar of spent coffee grounds

Ahmed S. El-Shafie[1] · Rehab Mahmoud[2] · Insharah Ahsan[1] · Helmi Hamdi[3] · Mohamed F. Shibl[4] · Marwa El-Azazy[1]

Received: 6 April 2023 / Accepted: 8 July 2024 / Published online: 29 August 2024

Abstract

Antibiotics are among the most widely used pharmaceutically active compounds. Possessing the capability to adversely impact the ecological system, existence of antibiotics in the environment is an escalating concern. With the purpose of removing two widely used antibiotics efficiently from aqueous solutions, the competency of two biochar (BC)-based sorbents derived from spent coffee (SC) grounds was investigated. Both pristine (SCBC) and nickel (II) oxide-impregnated (Ni-SCBC) biochars were utilized as sustainable and cost-effective sorbents to remove daunorubicin (DAYN) and tigecycline (TIGY) from single synthetic aqueous solutions and binary combinations. Batch adsorption experiments were controlled implementing Box–Behnken design. The removal efficiency of Ni-SCBC was superior compared to SCBC (TIGY: 67.06%, DAYN: 94.30%). Results of characterizations showed that impregnation with NiO changed the degree of crystallization with a remarkable increase in the surface area from 49.23 m^2/g in SCBC to 86.06 m^2/g in Ni-SCBC. Adsorption of DAYN and TIGY (single solutions) conformed well to Freundlich, and Langmuir isotherms, respectively. A maximum adsorption capacity (q_{max}) of 136.62 mg/g (DAYN) and 73.15 mg/g (TIGY) was reported in single solutions, compared to 23.50 mg/g (DAYN) and 58.42 mg/g (TIGY) in binary mixture. Adsorption kinetics onto Ni-SCBC fitted well with the pseudo-second-order (PSO) and Elovich models. Acquired results demonstrated that SCBC and Ni-SCBC are promising adsorbents for remedying antibiotics.

Keywords Metal oxide-decorated biochar · Pharmaceutical pollutants · Partially overlapped spectra · Box–Behnken design · Composite desirability function

Introduction

Pharmaceutically active compounds (PhACs) play critical roles in curing and deterring the different diseases, an issue which is of utmost importance to the quality of life. With an incessant consumption of PhACs both in veterinary and human rehearsals, a plethora of pharmaceuticals has been detected in wastewater. By and large, the source of PhACs could be the daily consumption, the industrial runoffs, and the medical waste from the point-of-care sewage (do

✉ Ahmed S. El-Shafie
aelshafie@qu.edu.qa

✉ Marwa El-Azazy
marwasaid@qu.edu.qa

Rehab Mahmoud
rehabkhaled@science.bsu.edu.eg

Insharah Ahsan
ia1803723@student.qu.edu.qa

Helmi Hamdi
hhamdi@qu.edu.qa

Mohamed F. Shibl
mfshibl@cu.edu.eg

[1] Department of Chemistry and Earth Sciences, College of Arts and Sciences, Qatar University, 2713 Doha, Qatar

[2] Chemistry Department, Faculty of Sciences, Beni-Suef University, Beni-Suef, Egypt

[3] Center for Sustainable Development, College of Arts and Sciences, Qatar University, 2713, Doha, Qatar

[4] Chemistry Department, Faculty of Sciences, Cairo University, Giza, Cairo 12613, Egypt

Amaral et al. 2019; El-Shafie et al. 2022; Lindberg et al. 2021; Majumder et al. 2021). The presence of PhACs has therefore arisen as a critical concern for the twenty-first century (Majumder et al. 2021). Generally, PhACs do not exist in the ecosystem as isolated entities. Rather, mixtures of drugs with different pharmacological actions and diverse chemical structures as well as their metabolites exist in the environment. The consequences on the ecosystem are greatly dependent on how complex this mixture is. Nonetheless, it is conceivable that these combinations could prompt serious ecotoxicological impacts depending on their individual effects and whether their interactions are of synergistic or antagonistic nature (do Amaral et al. 2019).

Daunorubicin (DAYN) is an antibiotic of the anthracycline family and is mostly used as anticancer to treat leukemia, breast, and ovarian cancers, lung carcinoma, as well as many sarcomas (Brel et al. 2021). The global DAYN market was approximated to be 1,959.95 million USD in 2021 and is anticipated to further expand to 3610.21 million USD by 2027 (Globenewswire 2022). The existence of DAYN in water (reported to be 26.0 ng/L in surface water) is attributed to the excretion of 13–15% of the DAYN dosage via urine within 24 h (Gouveia et al. 2019; Mahnik et al. 2007). TIGY is a novel tetracycline antibiotic (glycylcycline class) with a broad spectrum of activity and is an FDA-approved therapy for complicated skin and intra-abdominal infections. Tigecycline (TIGY) has been recently approved as a chemotherapeutic agent (Dong et al. 2019; El-Azazy et al. 2021a). TIGY is ranked the first in China and the second in the world, and its consumption in the USA has increased in the last two years from 3,000 to 3,200 tons (Daghrir and Drogui 2013). TIGY concentration in wastewater is 0.11 mg/L. The FDA has updated TIGY administration precautions to reflect the TIGY's increased mortality (FDA 2017).

Different approaches were used to remove DAYN and TIGY from synthetic and natural wastewater (Table S1). The growing need for economical and high-performance wastewater remediation systems has prompted scientists to explore green and sustainable solutions (Masanizan et al. 2021; Thotagamuge et al. 2021). Among the solutions is the recycling of agro-wastes into beneficial products. Biochar (BC) is a carbon-rich charcoal-like material that could be acquired from the pyrolysis of biomasses under oxygen-limited settings (Sun et al. 2021). Therefore, BC usually possesses a more significant concentration of recalcitrant carbon compared to the fresh parent biomass (Basak et al. 2022). The unique attributes of BC, including high surface area and porous structure, the existence of functionalities, stability, and liability for further functionalization, make it appropriate for innumerable environmental remediation purposes (Osman et al. 2022).

Coffee is a popular beverage worldwide. While preparing a beverage from one ton of coffee beans, ~ 0.65 tons of the grounds are wasted (Nguyen et al. 2021). Because brewing coffee uses just a tiny portion (0.2%) of the bean, vast quantities of waste are created from the ground beans globally. The spent coffee (SC) grounds are normally disposed of by burning or landfilling rather than composting or recycling. Alternative methods of disposing of SC grounds have been intensively researched to resolve these challenges. Since SC grounds are considered a potential energy source, it has been exploited to generate biodiesel and bioethanol (Shin et al. 2020).

In the current approach, the biochar of SC grounds (SCBC) will be recycled and further valorized into a value-added product for remediation of pharmaceutical wastewater. Furthermore, the impact of biochar surface modification with nickel oxide (NiO) nanoparticles on the removal capacity is explored. Nickel oxide (NiO)-impregnated biochar (Ni-SCBC) will be synthesized via the microemulsion-assisted method using oleylamine as a surfactant, which in turn helps forming small- and uniform-sized nanoparticles. Modification with the metal oxide nanoparticles aims to increase the surface area of the adsorbent and boost the number of active adsorption sites.

Most of the efforts for the treatment of DAYN or TIGY polluted wastewater were mainly focused on their single solutions and are mostly following a univariate-based scheme (Table S1) (Almufarij et al. 2022; El-Azazy et al. 2021a; El-Shafie et al. 2022; Ghodrati et al. 2022; Mello Souza et al. 2022; Sajedi and Moghaddas 2022; Zhong et al. 2022). Therefore, in the current investigation, we worked via two intermingling schemes. Since the purpose of the current approach is to generate a competent nanosorbent while maintaining the process sustainability and greenness, a multivariate approach—Box–Behnken design—was instigated to control the performance of the nanosorbent. Variables influencing the efficacy of Ni-SCBC as a nanosorbent (pH, Ni-SCBC dose (AD), pollutant concentration [Drug], and contact time (CT)) will be assessed. Two responses will be optimized: %removal (%R) and the adsorption capacity (q_e) (Tee et al. 2022). Following such a scheme helps lower the consumption of chemicals and preserve the resources, while obtaining trustworthy data.

By and large, the removal of DAYN and TIGY, like the other PhACs (Basheer 2018; El-Azazy et al. 2021a; Mansour et al. 2018; Rivera-Utrilla et al. 2013) (Table S1), was attempted from a single-component system with almost no attention being paid for the complicated nature of the pharmaceutical wastewater. Therefore, to mimic the actual situation and address this concern, removal of the two antibiotics from the multi-component solution has been undertaken in the current investigation. In this regard, Box–Behnken design was fully exploited: first to sustainably tune the variables' levels that could maximize the removal of both drugs from their individual solutions, and moreover to apply the

Derringer's composite desirability (D) tool to boost the uptake of both drugs simultaneously. Parallel to that, the interfacial effects of the biochar and the biochar-based composite adsorbents and the microstructural changes triggered by the loading of NiO are still worth investigation. In the same itinerary, comprehending the impact of existence of one antibiotic on another antibiotic and the competition on the active adsorption sites was explored in depth using different equilibrium isotherm and kinetic models. As far as is known, this is the first investigation targeting the remediation of two antibiotics that are extensively used nowadays from their mixture employing statistical analysis and modeling with no need to instigate a preceding chemical or graphical treatment.

Materials and methods

Materials

Analytical-grade materials were used throughout the investigation. Sodium tetraborate-10-hydrate ($Na_2B_4O_7{\cdot}10H_2O$), sodium hydroxide, hydrochloric acid, sulfuric acid, ethanol, sodium carbonate, sodium chloride, nickel (II) nitrate hexahydrate ($Ni(NO_3)_2{\cdot}6H_2O$), and the tested dyes (rose bengal, fuchsine, and methylene blue) were bought from Sigma-Aldrich (USA). Biosynth® Carbosynth Ltd. (UK) was the source for both daunorubicin hydrochloride (DAYN, $C_{27}H_{29}NO_{10}{\cdot}HCl$, M_r: 563.98 g/mol, purity (reported method): min. 95%) and tigecycline (TIGY, $C_{29}H_{39}N_5O_8$, M_r: 585.65 g/mol, purity (HPLC): min. 98 area-%), as well as the drugs used in the selectivity test (rifampicin, riboflavin, marbofloxacin, amantadine, sofosbuvir). The ultrapure deionized water was secured from the Millipore-Q water system. Powdered coffee was obtained from the local markets.

Preparation of the adsorbents

Spent coffee (SC) grounds were acquired by boiling the coffee powder in hot tap water 5 times, and then, the residual solid SC grounds were washed 5 times with tap water and then 10 times with deionized water. The clean SC grounds were then roasted for 3 days at 80 °C before crushing and sieving using 0.125 mm sieve. The product was placed in porcelain crucibles (Coors™, Merck, USA), which were then firmly sealed, and burnt in the furnace at 500 °C for 1 h, and the yield was marked as spent coffee grounds biochar (SCBC). To prepare the Ni-SCBC, NiO nanoparticles were produced using the microemulsion method with slight adjustments (Bumajdad et al. 2004). The Ni-SCBC was produced by dissolving 3.3225 ± 0.0005 g of ($Ni(NO_3)_2{\cdot}6H_2O$) in 200 mL of deionized water (equal to 1:10 Ni: SCBC, wt/wt%) followed by adding 10 g of the SCBC while stirring continuously at 750 rpm. A volume of 100 mL of oleylamine (0.1 M) dissolved in 2-propanol was added to the previous solution, and the mixture was agitated for 3 h. The formation of NiO nanoparticles was accomplished by adding drops of 26% ammonia solution gradually until the pH is ~ 12. The product, Ni-SCBC, was separated by centrifugation at 4000 rpm for 5 min. The product was then washed with deionized water followed by absolute ethanol 5 times and then dried in the oven at 70 °C for 24 h.

Box–Behnken design

Box–Behnken design was prompted to maximize the efficiency of the Ni-SCBC in removing DAYN and TIGY. The design was formulated and analyzed using Minitab®19, Minitab Inc. The pH, drug concentration [Drug], the dosage of Ni-SCBC (AD), and contact duration (CT) were the four key parameters investigated (Table 1). (The lower bound is symbolized as − 1, and the upper bound is symbolized as + 1.)

Generally, a 500-ppm stock solution was prepared by dissolving the necessary quantities of TIGY and DAYN in deionized water. Drug concentrations in Table 2 were secured via serial dilutions. An adsorbent mass as per the specifications mentioned in Table 2 was mixed with the appropriate drug concentration, and the pH was then adjusted using 0.1 M aqueous solution of either sodium hydroxide or hydrochloric acid to achieve the target pH ± 0.2. The reaction mixture was left in the shaker at 160 rpm for the specified times (Table 2). Samples were then filtered, and the absorbance of the filtrate was reckoned using a UV–Vis spectrophotometer (Agilent diode-array, Agilent, USA) at λ_{max} values of 347 nm and 478 nm for TIGY and DAYN, respectively.

Equations (1) and (2) were used to compute the two responses to be optimized in this investigation, $\%R$ and q_e (mg/g). The design scheme consisted of 27 trials including 3 central points (Ct Pt, denoted as 0). The design was carried out as 3 blocks, as demonstrated in Table 2.

$$(\%R) = \frac{C_0 - C_e}{C_0} \times 100\% \tag{1}$$

$$(q_e) = \frac{C_0 - C_e}{W} \times V \tag{2}$$

Table 1 Studied factors and their levels

Variables and Units	− 1	0	+ 1
pH (*A*, pH Unit)	5.0	7.0	9.0
Ni-SCBC Amount (AD, *B*, mg/thirteen mL)	10.0	45.0	80.0
Drug Concentration ([Drug], *C*, ppm)	20.0	60.0	100.0
Reaction duration (CT, *D*, min)	10.0	65.0	120.0

Table 2 Design matrix for the removal of TIGY and DAYN from their single solutions. Experimental, and predicted (theoretical) values, as well as the % error (%Er) for the two responses, are shown

Run #	Blk	Variables				DAYN						TIGY					
		pH	AD	[Drug]	CT	$\%R_{exp}$	$\%R_{prd}$	%Er	$q_{e\ exp}$	$q_{e\ prd}$	%Er	$\%R_{exp}$	$\%R_{prd}$	%Er	$q_{e\ exp}$	$q_{e\ prd}$	%Er
01	1	7(0)	45(0)	100(+)	120(+)	46.93	46.54	0.84	13.56	13.52	0.30	49.90	50.54	1.27	14.42	15.10	4.50
02	1	7(0)	45(0)	100(+)	10(−)	44.27	43.95	0.73	12.79	12.81	0.16	50.80	51.74	1.82	14.65	15.25	3.93
03	1	9(+)	80(+)	60(0)	65(0)	61.90	61.75	0.24	6.04	6.03	0.17	60.21	62.11	3.06	5.88	6.25	5.92
04	1	5(−)	80(+)	60(0)	65(0)	94.30	93.75	0.59	9.19	8.43	9.02	62.75	64.35	2.49	6.12	6.14	0.33
05	1	7(0)	45(0)	20(−)	120(+)	63.30	62.82	0.76	3.66	3.50	4.57	45.14	46.70	3.34	2.62	2.36	11.02
06	1	9(+)	10(−)	60(0)	65(0)	50.58	49.92	1.32	39.46	40.98	3.71	47.73	48.86	2.31	37.23	37.14	0.24
07	1	7(0)	45(0)	60(0)	65(0)	58.57	57.49	1.88	10.15	10.00	1.50	59.51	60.60	1.80	10.31	10.50	1.81
08	1	7(0)	45(0)	20(−)	10(−)	61.35	60.90	0.74	3.55	3.41	4.11	42.18	43.97	4.07	2.44	2.16	12.96
09	1	5(−)	10(−)	60(0)	65(0)	49.13	48.54	1.22	38.32	37.41	2.43	55.79	56.69	1.59	43.49	42.45	2.45
10	3	7(0)	10(−)	60(0)	120(+)	49.93	52.48	4.86	38.94	40.64	4.18	48.09	49.58	3.01	37.51	38.46	2.47
11	3	5(−)	45(0)	20(−)	65(0)	57.82	60.76	4.84	3.34	3.60	7.22	47.38	48.56	2.43	2.74	2.66	3.01
12	3	9(+)	45(0)	20(−)	65(0)	60.98	64.49	5.44	3.52	3.53	0.28	48.93	49.64	1.43	2.83	2.69	5.20
13	3	7(0)	10(−)	60(0)	10(−)	44.45	46.06	3.50	34.67	35.74	2.99	47.19	48.01	1.71	36.78	37.71	2.47
14	3	7(0)	45(0)	60(0)	65(0)	53.80	57.49	6.42	9.32	10.00	6.80	59.14	60.60	2.41	10.26	10.50	2.29
15	3	7(0)	80(+)	60(0)	10(−)	71.14	75.34	5.57	6.94	7.22	3.88	57.91	58.89	1.66	5.65	05.58	1.25
16	3	9(+)	45(0)	100(+)	65(0)	41.78	42.81	2.41	12.07	12.36	2.35	48.47	49.66	2.40	14.00	14.63	4.31
17	3	5(−)	45(0)	100(+)	65(0)	47.07	48.67	3.29	13.60	14.78	7.98	59.05	60.90	3.04	17.05	17.91	4.80
18	3	7(0)	80(+)	60(0)	120(+)	64.54	67.68	4.64	6.30	6.66	5.41	57.29	58.98	2.87	5.58	5.51	1.27
19	2	7(0)	80(+)	20(−)	65(0)	68.27	65.24	4.64	2.22	2.29	3.06	51.88	48.81	6.29	1.69	2.02	16.34
20	2	9(+)	45(0)	60(0)	120(+)	64.85	61.69	5.12	11.24	10.80	4.07	53.23	50.61	5.18	9.23	8.86	4.18
21	2	5(−)	45(0)	60(0)	120(+)	57.83	55.60	4.01	10.02	09.81	2.14	66.06	62.93	4.97	11.45	11.40	0.44
22	2	7(0)	10(−)	20(−)	65(0)	63.90	60.34	5.90	16.61	16.31	1.84	47.23	44.91	5.17	15.50	16.40	5.49
23	2	7(0)	45(0)	60(0)	65(0)	60.90	57.49	5.93	10.56	10.00	5.60	63.20	60.91	3.76	10.94	10.50	4.19
24	2	7(0)	10(−)	100(+)	65(0)	39.68	38.96	1.85	51.58	48.45	6.46	46.91	45.07	4.08	60.98	58.20	4.78
25	2	5(−)	45(0)	60(0)	10(−)	67.01	63.59	5.38	11.61	11.49	1.04	57.22	54.68	4.65	9.91	9.94	0.30
26	2	9(+)	45(0)	60(0)	10(−)	50.54	49.23	2.66	8.76	8.50	3.06	59.14	56.75	4.21	10.25	9.94	3.12
27	2	7(−)	80(+)	100(+)	65(0)	60.34	58.39	3.34	9.81	9.49	3.37	63.87	61.02	4.67	7.83	6.90	13.48

Blk: Block, Prd: predicted (theoretical) value, Exp: experimental value, $\%\ \mathrm{Er} = \left| \frac{Theoretical(Predicted)Value - ExperimentalValue}{Theoretical(Predicted)Value} \right| \times 100$

where C_0 is the initial concentration of either drug ([TIGY] and [DAYN]) in ppm, C_e is the equilibrium concentration of these two pharmaceutical solutions (ppm), V is the volume of TIGY and DAYN solution (L), and W is the weight of the Ni-SCBC.

Removal of TIGY and DAYN from binary mixture—analysis of the partially overlapped spectra

The removal of TIGY and DAYN from their bicomponent solution was investigated using Derringer's composite desirability function (D), as illustrated in Eq. (3). Desirability function is a multiple response optimization tool offered by Minitab® to find the ideal experimental conditions to maximize the removal of both drugs.

$$D = \left(d_1^{r1} d_2^{r2} \ldots d_m^{rm}\right)^{\frac{1}{\sum ri}} = \left(\prod_{i=1}^{n} d_1^{ri}\right)^{\frac{1}{\sum ri}} \quad (3)$$

where D is the composite desirability function, d is the individual desirability, r is the significance of each response, and m is the number of responses to be optimized. The responses in the current study are $\%R$ and q_e for both TIGY and DAYN. Individual spectra of TIGY and DAYN revealed maximum absorbances at λ_{max} values of 347 nm and 478 nm, respectively, suggesting a case of partially overlapped spectra (Fig. S2) (El-Shafie et al. 2024). Equations (4) and (5) were solved to determine the concentrations of TIGY

and DAYN in their binary mixture before and after their treatment using the Ni-SCBC nanosorbent.

$$A_{347} = \varepsilon_{\text{TIGY }347}.[\text{TIGY}] + \varepsilon_{\text{DAYN }347}.[\text{DAYN}] \quad (4)$$

$$A_{478} = \varepsilon_{\text{TIGY }478}.[\text{TIGY}] + \varepsilon_{\text{DAYN }478}.[\text{DAYN}] \quad (5)$$

Assuming that the path length is 1 cm, the values A_{347} and A_{478} represent the absorbance of either TIGY or DAYN measured at both λ_{max} values. The constants $\varepsilon_{TIGY347}$, $\varepsilon_{DAYN347}$, $\varepsilon_{TIGY478}$, and $\varepsilon_{DAYN478}$ were calculated by measuring the absorbance of TIGY and DAYN standard solutions separately at the two wavelengths. [TIGY] and [DAYN] are the concentrations of TIGY and DAYN to be determined. A calibration curve was prepared at each wavelength for both [TIGY] and [DAYN], and the slopes of the curves were used to calculate the ε values. Equations (4) and (5) were solved for the unknown [TIGY] and [DAYN] operating the matrices in Eqs. (6) and (7), respectively. Regression equations were used to obtain the slope and the molar absorptivity (Table 3).

$$[\text{TIGY}] = \frac{\begin{bmatrix} A_{347} & \varepsilon_{\text{DAYN }347} \\ A_{478} & \varepsilon_{\text{DAYN }478} \end{bmatrix}}{\begin{bmatrix} \varepsilon_{\text{TIGY }347} & \varepsilon_{\text{DAYN }347} \\ \varepsilon_{\text{TIGY }478} & \varepsilon_{\text{DAYN }478} \end{bmatrix}} = \frac{A_{347} \cdot \varepsilon_{\text{DAYN }478} - A_{478} \cdot \varepsilon_{\text{DAYN }347}}{\varepsilon_{\text{TIGY }347} \cdot \varepsilon_{\text{DAYN }478} - \varepsilon_{\text{TIGY }478} \cdot \varepsilon_{\text{DAYN }347}} \quad (6)$$

$$[\text{DAYN}] = \frac{\begin{bmatrix} \varepsilon_{\text{TIGY }347} & A_{347} \\ \varepsilon_{\text{TIGY }478} & A_{478} \end{bmatrix}}{\begin{bmatrix} \varepsilon_{\text{TIGY }347} & \varepsilon_{\text{DAYN }347} \\ \varepsilon_{\text{TIGY }478} & \varepsilon_{\text{DAYN }478} \end{bmatrix}} = \frac{\varepsilon_{\text{TIGY }347} \cdot A_{478} - \varepsilon_{\text{TIGY }478} \cdot A_{347}}{\varepsilon_{\text{TIGY }347} \cdot \varepsilon_{\text{DAYN }478} - \varepsilon_{\text{TIGY }478} \cdot \varepsilon_{\text{DAYN }347}} \quad (7)$$

Characterization

The structural features of SCBC and Ni-SCBC were analyzed operating a scanning electron microscope (SEM, FEI, Quanta 200, Thermo Scientific, USA). Energy-dispersive X-ray spectrometer (EDX) was operated to explore the elemental structure of both adsorbents. Inductively coupled plasma–optical emission spectrometry (ICP-OES, Optima 7300 DV, PerkinElmer, USA) was employed to verify the amount of nickel loaded on the biochar. The Ni-SCBC sample was prepared for the ICP-OES analysis via the acid digestion method, where 0.25 g of the sample was placed into the digestion vessel followed by 6 mL of nitric acid, 2 mL of hydrochloric, and hydrofluoric concentrated acids. The vessel was then digested in the microwave digestor (MARS 6CM, USA) for 15 min using the power of 1800 W. The vessel was left to cool down for another 15 min. After digestion, the sample solution was neutralized to pH 7 using NaOH solution and the volume was diluted to 100 mL using deionized water. Transmission electron microscopy (TEM) was used to analyze the microstructure of SCBC before and after loading by NiO nanoparticles (TECNAI G2 TEM, TF20, FEI, USA). A porosimetry system, Micrometrics ASAP2020™ (Micrometrics, USA), was employed to investigate the surface properties, including pore size, volume, and the area of the adsorbent surface. Analysis was done by degassing of the SCBC and Ni-SCBC samples, followed by N_2 adsorption–desorption investigation. The *t*-plots, on the other hand, were utilized in conjunction with the Barrett–Joyner–Halenda (BJH) equations to calculate the pore volume (Bumajdad et al. 2004; Mansour et al. 2018). Thermogravimetric analysis (TGA/*d*TA) was performed at a temperature range of 50–800 °C using TGA/*d*TA (TGA, PerkinElmer-TGA400, USA). Raman spectroscopy was used to explore the carbonaceous nature of both SCBC and Ni-SCBC using a DXR3 Raman Microscope (Thermo Fischer Scientific, wavelength of 532 nm, 40 times scanning, laser power of 9.2 mW). Fourier transform infrared

Table 3 Molar absorptivity values for the binary mixture components that were obtained from the calibration curves and analyzed at λ_{max} values

Drug/λ_{max} (nm)	Regression equation (y = *m*x + *b*)	Slope (*m*, ε_{Drug}, L.mol^{-1}.cm^{-1})	R^2
DAYN, 347	$y = 1049.7x + 0.0324$	1049.7	0.9928
DAYN, 487	$y = 6838.5x + 0.1983$	6838.5	0.9935
TIGY, 347	$y = 8849x - 0.1035$	8849.0	0.9551
TIGY, 487	$y = 1755.2x - 0.0235$	1755.2	0.9378

(FT-IR) spectroscopic analysis (Spectrum 400 FT-IR, PerkinElmer, USA) was used to investigate the functional groups that exist on the surface of both SCBC and Ni-SCBC as well as DAYN and TIGY prior to and following the adsorption. The pH_{PZC} for SCBC and Ni-SCBC was evaluated by adding sodium chloride (0.01 M) aqueous solution and following the previously described procedure (Babic et al. 1999; Kooh et al. 2018).

Equilibrium and kinetic investigations

To investigate the adsorption equilibrium for single and binary drug solutions, a series of dilutions ranging from 5 to 400 ppm of the drug(s) solutions was prepared using deionized water and the pH was adjusted to 5.0 ± 0.2. Each drug solution was mixed with 0.1000 ± 0.0005 g of Ni-SCBC. An automatic shaker was used to shake the drug–adsorbent combination for 24 h at 160 rpm. The produced solutions were filtered, and the absorbance was measured at the λ_{max} value for each drug. The residual drug concentration in the binary system was determined using Eqs. (6) and (7).

The adsorption kinetics for TIGY and DAYN were evaluated by adding 150 mL (100 ppm, pH 5.0 ± 0.2) of both drug solutions to a mass of 0.5000 ± 0.0005 g of Ni-SCBC, stirred continuously at 160 rpm. Over 90 min, aliquots of 10 mL of the reaction mixture were taken and filtered at various time intervals. Lastly, the absorbance of the filtrate was detected.

Selectivity of Ni-SCBC

To determine the selectivity of the prepared adsorbent, Ni-SCBC for DAYN and TIGY, the removal efficiency of Ni-SCBC toward these two drugs was compared with that toward five other drugs (rifampicin, riboflavin, marbofloxacin, amantadine, and sofosbuvir) as well as three dyes (rose bengal, fuchsine, and methylene blue) (Cantarella et al. 2019). Specifically, 13 mL aliquots of each contaminant with a concentration of 50 ppm was mixed with 0.100 ± 0.005 g of Ni-SCBC, and the pH of each contaminant solution was adjusted to 5.0 ± 0.2 using 0.1 M aqueous HCl. The mixture was stirred at 150 rpm for 2 h and filtered, and the filtrate's absorbance was recorded at λ_{max} of each adsorbate solution.

Desorption and regeneration of Ni-SCBC

To investigate the possibility of adsorbent reusability, a mass of the adsorbent Ni-SCBC (1.0000 ± 0.0005 g) was first equilibrated with 150 mL of 50 ppm from both DAYN, TIGY, and their binary mixture for 2 h followed by filtration. The adsorbent was then rinsed with deionized water to eliminate any non-adsorbed remnants of the two drugs before being dried in the oven at 70 °C for 24 h. Five different eluents were employed in this investigation, including: 0.1 M of hydrochloric acid, sulfuric acid, sodium carbonate, 10% ethanol, and deionized water. In the desorption experiment, 0.1000 ± 0.0005 g of the drug-loaded adsorbent was mixed with 10 mL of each eluent. The samples were shaken for 60 min, followed by filtration using syringe filters. Each desorption experiment was conducted 3 times, and the average desorbed quantity was recorded. The standard deviation of the multiple measurements was expressed using error bars.

The recovery experiments were performed by using 0.1 M sulfuric acid for DAYN, 0.1 M hydrochloric acid for TIGY, and 0.1 M sulfuric acid for the desorption of the two drugs in the binary mixture. For 30 min, an amount of 0.2000 ± 0.0005 g of Ni-SCBC was equilibrated with 50 mL of 50 ppm drug solution (pH 5.0 ± 0.2). The resulting mixture was then filtered, and the absorbance was determined. The loaded adsorbent was eluted with chosen eluent, and samples were then dried at 70 °C for 1 h before being employed in another adsorption cycle. This method was repeated 6 times, and the removal efficiency (%*R*) was calculated following each cycle.

Results and discussion

Adsorption study

Findings of the preliminary experiments

The performance of the two adsorbents, SCBC and Ni-SCBC, was initially screened and compared using un-optimized experimental conditions. Table 4 shows that the Ni-SCBC has a better performance compared to the pristine candidate, SCBC. Therefore, Ni-SCBC will be the adsorbent of choice to be used throughout this work.

Table 4 Comparison of the efficiency of SCBC and Ni-SCBC toward the removal of DAYN and TIGY. Experimental conditions were unified (un-optimized) as follows: pH = 7, adsorbent dose (AD) = 100 mg, [Drug] = 100 mg/L, and contact time (CT) = 60 min. Measurements of the remaining drug concentrations were taken at 478 and 347 nm for DAYN and TIGY, respectively

Adsorbent	$\%R_{DAYN}$	$\%R_{TIGY}$	$q_{e\ DAYN}$ (mg/g)	$q_{e\ TIGY}$ (mg/g)
SCBC	14.78	25.25	1.92	3.28
Ni-SCBC	48.63	40.16	6.32	5.22

Design of the experiments: Box–Behnken design

Box–Behnken design is one of the response surface methodology-based factorial designs. Compared to the other response surface designs, Box–Behnken design entails fewer experimental points with no contributions from the preceding screening design (Box and Behnken 1960; Tee et al. 2022). In the current investigation, the obtained data were fitted to the polynomial paradigm defined by Eq. (8).

$$y = a_0 + \sum_{i=1}^{n} a_i x_i + \sum_{i=1}^{n} \sum_{j=i+1}^{n} b_{ij} x_i x_j + \sum_{i=1}^{n} \sum_{j=i+1}^{n} \sum_{k=j+1}^{n} c_{ijk} x_i x_j x_k \tag{8}$$

In this model, y represents the theoretic response variable ($\%R$ or q_e (mg/g)), a_0 signifies the global mean, while x_i, x_j, *and* x_k are the independent factors, and the coefficients: a_i, b_{ij}, *and* c_{ijk} represent the effects of a single-factor, two-factor, and three-factor interactions, respectively. To improve the response modelling, data transformation was conducted using the Box–Cox response transformation tool, as shown in Eq. (9), where λ represents the transformation factor (Box and Cox 1964).

$$y^{(\lambda)} = \begin{cases} \frac{y^{\lambda}-1}{\lambda} & \lambda \neq 0 \\ \log(y) & \lambda = 0 \end{cases} \tag{9}$$

In the current investigation, the trail of the adsorption experiments involving the use of Ni-SCBC was evaluated in accordance with the settings exhibited in Table 2.

Screening phase

The Pareto chart was used to comprehend the influence of each variable as well as variable–variable linear and squared interactions on the measured response(s) (Fig. 1a, b). As shown in Fig. 1a, b, for both drugs and assessing the influence of the main effects on $\%R$, the [Drug] (C) and the dose of Ni-SCBC (B) were the most significant variables affecting the removal efficiency, implying that the dose of the adsorbent and the [Drug] play the major role in shaping the adsorption process. Main effects plot (figure is not shown) reveals that as the dose of the adsorbent (Ni-SCBC) increases, the $\%R$ of either drug increases. A higher dose of the adsorbent implies an availability of more active adsorption sites for capturing the drug. In the case of TIGY, the same plot shows that the adsorption increases as the [TIGY] increases till a concentration of ~ 70–85 ppm; then, the $\%R$ starts to decline implying the saturation of the adsorption sites at higher concentrations. The same was noted in the case of DAYN; however, the adsorption starts to decline at ~ 20–30 ppm of the drug.

The pH (A) was the third main effect in terms of statistical significance. Main effects plot shows that as the pH increases, the $\%R$ of either drug decreases. This finding will be further explained in relation to the pK_a of the drug and the pH_{pzc} of the adsorbent. While the CT (D) was the least statistically significant factor for both drugs, the squared effect (DD) was statistically significant in the case of TIGY and insignificant in the case of DAYN. The impact of linear and squared interactions could be deduced from the Pareto chart.

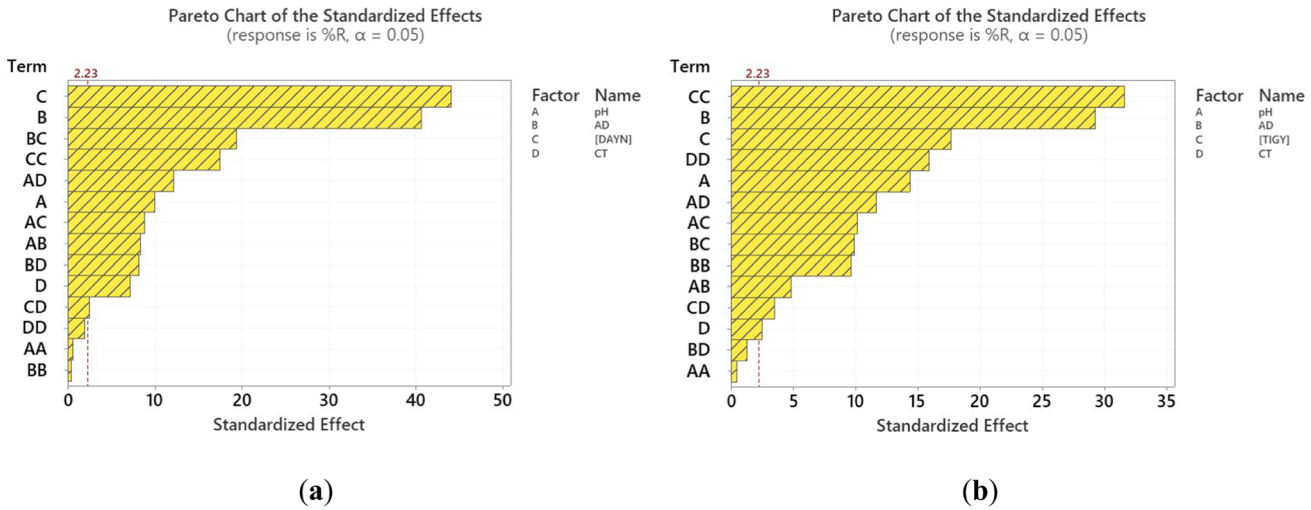

Fig. 1 Pareto chart demonstrating the impact of the experimental conditions on the $\%R$ from single drug solutions: **a** $\%R_{DAYN}$, **b** $\%R_{TIGY}$

Statistical models and analysis of variance (ANOVA)

The regression models derived for both drugs are described in Eqs. (10–13). These models demonstrate the relationship between the responses and the various experimental conditions. Unlike the Pareto charts, these models explain the size and direction of the variable's influence. As a result, the total influence of any element may be simply determined using these models. Noteworthy, the optimum responses were attained operating the Box–Cox response transformation (Menazea et al. 2020). In the case of DAYN and the mixture of DAYN and TIGY, the value of λ (transformation factor) was selected to be 'optimal' compared to 0.5 in the case of TIGY.

$$\begin{aligned}(\%R^{\lambda-1})/\left(\lambda \times g^{(\lambda-1)}\right)_{(\mathrm{DAYN})} &= 456329 + 1.61\,\mathrm{pH} + 0.4151\,\mathrm{AD} + 0.2435\,[\mathrm{DAYN}] \\ &- 0.2112\,\mathrm{CT} - 0.0550\,\mathrm{pH}^2 - 0.000126\,AD^2 - 0.003995 \\ &[\mathrm{DAYN}]^2 - 0.000239\,\mathrm{CT}^2 - 0.05064\,\mathrm{pH} \times \mathrm{AD} \\ &- 0.04678\,\mathrm{pH} \times [\mathrm{DAYN}] + 0.04671\,pH \times \mathrm{CT} + 0.005860\,\mathrm{AD} \times \\ &[\mathrm{DAYN}] - 0.001806\,\mathrm{AD} \times \mathrm{CT} + 0.000477\,[\mathrm{DAYN}] \times \mathrm{CT}, (\lambda \\ &= -2.45103,\ g = 56.5862 \text{ is the geometric mean of } \%R)\end{aligned} \tag{10}$$

$$\begin{aligned}q^{\lambda}_{e\,(\mathrm{DAYN})} &= 1.4508 - 0.0092\ \mathrm{pH} - 0.010507\ \mathrm{AD} + 0.008592\,[\mathrm{DAYN}] \\ &- 0.000845\ \mathrm{CT} + 0.000904\ \mathrm{pH}^2 + 0.000088\ \mathrm{AD}^2 \\ &- 0.000041\,[\mathrm{DAYN}]^2 - 0.000001\ \mathrm{CT}^2 - 0.000300\ \mathrm{pH} \times \\ &\mathrm{AD} - 0.000101\ \mathrm{pH} \times [\mathrm{DAYN}] + 0.000173\ \mathrm{pH} \times \mathrm{CT} \\ &+ 0.000001\ \mathrm{AD} \times [\mathrm{DAYN}] - 0.000006\ \mathrm{AD} \times \mathrm{CT} \\ &+ 0.000001\,[\mathrm{DAYN}] \times \mathrm{CT},\ (\lambda = 0.138702)\end{aligned} \tag{11}$$

$$\begin{aligned}\sqrt{\%\mathrm{R}^{\lambda}_{(\mathrm{TIGY})}} &= 4.135 + 0.1774\ \mathrm{pH} + 0.00468\ \mathrm{AD} + 0.06110\,[\mathrm{TIGY}] \\ &+ 0.03050\ \mathrm{CT} - 0.00204\ \mathrm{pH}^2 - 0.000140\ \mathrm{AD}^2 \\ &- 0.000350\,[\mathrm{TIGY}]^2 - 0.000093\ \mathrm{CT}^2 + 0.001423\ \mathrm{pH} \\ &\times \mathrm{AD} - 0.002606\ \mathrm{pH} \times [\mathrm{TIGY}] - 0.002177\ \mathrm{pH} \times \mathrm{CT} \\ &+ 0.000145\ \mathrm{AD} \times [\mathrm{TIGY}] - 0.000014\ \mathrm{AD} \\ &\times \mathrm{CT} - 0.000033[\mathrm{TIGY}] \times \mathrm{CT}\end{aligned} \tag{12}$$

$$\begin{aligned}\sqrt{q^{\lambda}_{e\,(\mathrm{TIGY})}} &= 3.648 - 0.084\ \mathrm{pH} - 0.12237\ \mathrm{AD} + 0.09144\,[\mathrm{TIGY}] \\ &+ 0.01213\ \mathrm{CT} + 0.0071\ \mathrm{pH}^2 + 0.000920\ \mathrm{AD}^2 - 0.000273 \\ &[TIGY]^2 - 0.000035\,CT^2 + 0.001584\ \mathrm{pH} \times \mathrm{AD} - 0.001296\ \mathrm{pH} \\ &\times [\mathrm{TIGY}] - 0.000909\ \mathrm{pH} \times \mathrm{CT} - 0.000424\ \mathrm{AD} \\ &\times [\mathrm{TIGY}] - 0.000010\ \mathrm{AD} \times \mathrm{CT} - 0.000010\,[\mathrm{TIGY}] \times \mathrm{CT}\end{aligned} \tag{13}$$

Table 5 displays summaries of the four models. Every model was evaluated considering three parameters: the coefficient of determination (R^2), the R^2 adjusted (R^2-adj), and the R^2 predicted (R^2-pred). The model's linearity was assessed using the values of R^2 and R^2-adj. As per Table 5, both parameters had high values, suggesting that both models were linear. The R^2-pred measures the model's capacity to predict the response to new trials. The

Table 5 Parameters used to assess the regression equations for the removal of the single drug solutes, Eqs. (10–13), and the optimum conditions

Contaminant	Response	R^2%	R^2-adj%	R^2-pred	Optimum Conditions, Desirability (d) Values, and Predicted Performance Indicators
DAYN	$\%R$	99.80	99.48	98.61	pH = 5, AD = 80 mg, [DAYN] = 24.33 ppm, CT = 10 min, (d = 1.000, $\%R$ = 99.60%)
	q_e	99.88	99.68	99.00	pH = 9, AD = 10 mg, [DAYN] = 94.34 ppm, CT = 120 min, (d = 1.000, q_e = 57.58 mg/g)
TIGY	$\%R$	99.69	99.19	97.39	pH = 5, AD = 80 mg, [TIGY] = 81.41 ppm, CT = 84.44 min, (d = 1.000, $\%R$ = 67.74%)
	q_e	99.79	99.45	98.21	pH = 5, AD = 10 mg, [TIGY] = 100.0 ppm, CT = 93.33 min, (d = 1.000, q_e = 63.00 mg/g)

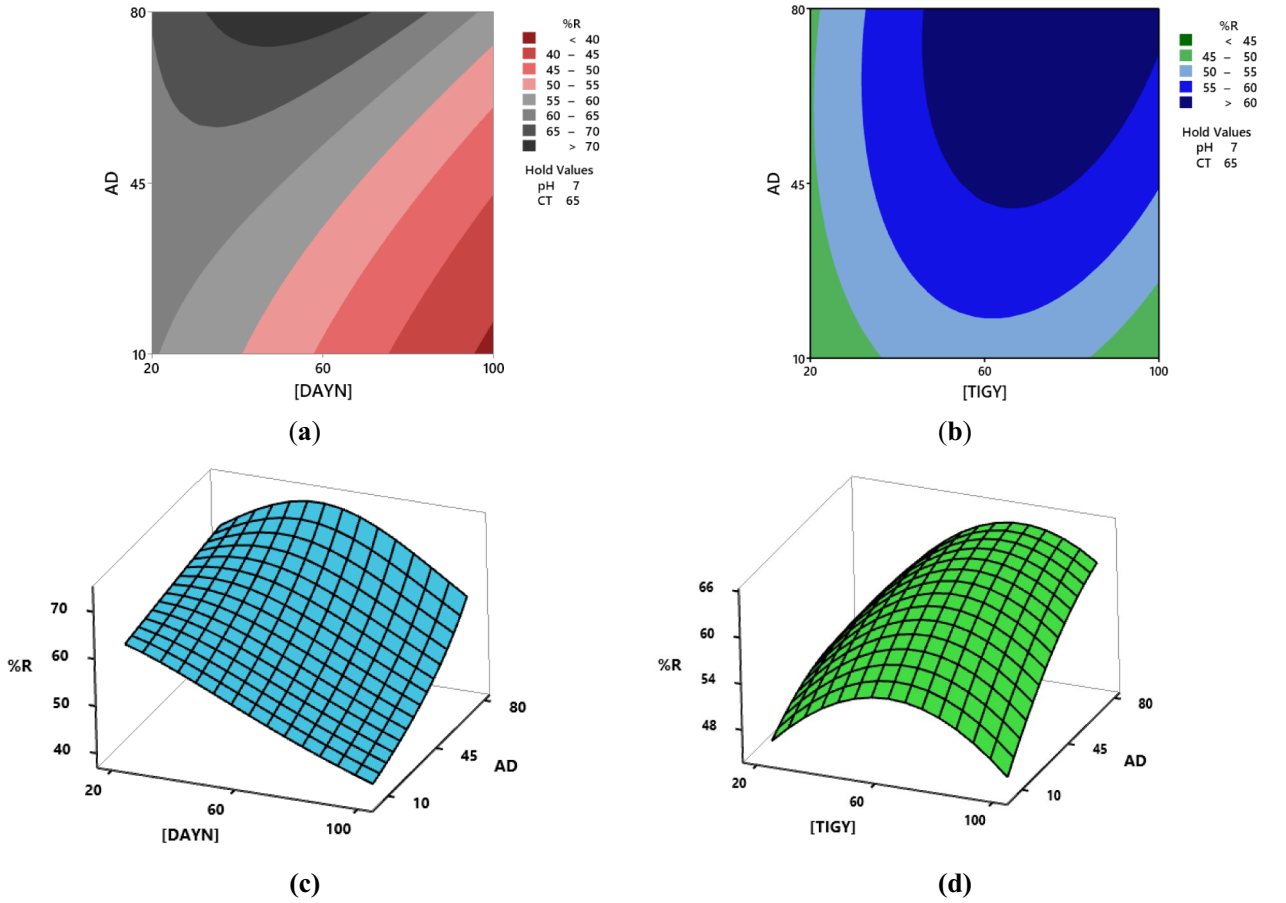

Fig. 2 Two-dimensional contour plot; **a** *%R* vs AD, [DAYN], **b** *%R* vs AD, [TIGY], three-dimensional surface plot; **c** *%R* vs AD, [DAYN], and **d** *%R* vs AD, [TIGY]

high values of R^2-pred indicate stronger model capability. The %Er was used to analyze the difference between experimental and theoretical (predicted) values. The %Er values were relatively minimal, indicating that the experimental and the theoretical values agreed well (Table 2). Following this step, the ANOVA test at a confidence level of 95.0 was used—tables are not presented. A factor with a *p*-value of $^{>}$ 0.05 was deemed statistically insignificant. The ANOVA results aligned well with the findings drawn from the regression equations and Pareto charts.

Optimization of the individual responses

Following the screening phase, an optimization step was contemplated utilizing the 2D contour and 3D surface plots. Figure 2a–d presents the contour and the surface plots considering the *%R* as a response. Figure 2a, b depicts the contour plots in the case of DAYN and TIGY, respectively. The dark gray (Fig. 2a) and dark blue (Fig. 2b) regions represent the zone where the joint effect of both variables reaches the highest $\%R_{\mathrm{DAYN}}$ and $\%R_{\mathrm{TIGY}}$, respectively. The 2D plot and as could be deduced from Fig. 2a, b relates two variables to *%R*. As shown, the interaction of the most significant variables (AD, [Drug]) was depicted. In general, increasing the AD is accompanied by a better removal performance, however, dependent on [Drug]. In the case of TIGY, for example, a 60 ppm of TIGY could be removed with an efficiency > 60% using a dose of ~ > 45–80 mg of Ni-SCBC. Figure 2c, d illustrates the surface plots of the same two variables investigated and the *%R*. The elevated edges shown in both figures represent the point of the maximum *%R*. For both drugs, as the dose of Ni-SCBC increases, the removal increases, however, dependent on the [Drug]. For example, a low uptake of TIGY could be noted at the very low and the very high [TIGY]. Other tools such as the individual desirability value (*d*)—figures are not shown (Table 5)—were utilized as a signal for the best factorial blend, where the greater the value of *d*, the better the specified blend and the higher the response.

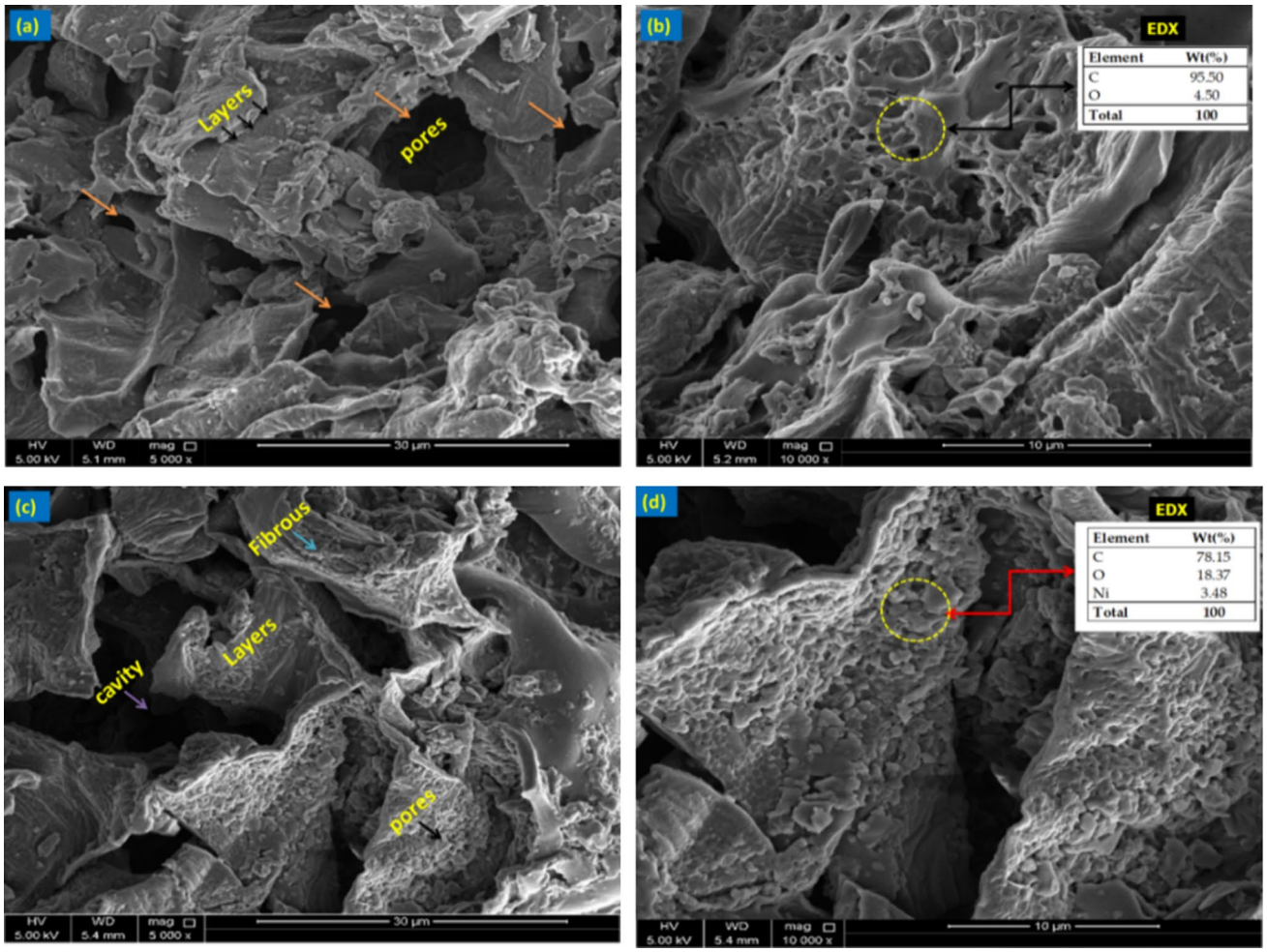

Fig. 3 SEM micrographs of **a, b** SCBC, **c, d** Ni-SCBC at various magnifications 5,000×and 10,000×, and **b, d** the inset tables represent the EDX analysis data of SCBC and Ni-SCBC, respectively

Multi-response optimization: Multi-component drug solution

Figure S1 is utilized to determine the ideal parameters that would maximize the observed responses simultaneously in the case of the bicomponent drug solution. Similar to the individual desirability value (*d*), the value of the composite desirability function (*D*) was used to indicate the suitability of the shown factorial blend for boosting the *%R* of both drugs concurrently. The *D*-function obtained for $\%R_{DAYN}$ and $\%R_{TIGY}$ simultaneously is shown in Fig. S1. The optimum parameters (denoted as '*Curr*') with a *D*-value of 0.9899 were obtained using pH 5.0, AD of 80 mg, [DAYN] of 83.03 ppm, and CT of 51.11 min. Considering these optimum conditions, the removal efficiencies of DAYN and TIGY are 94.4%, and 65.6%, respectively. Therefore, in a binary mixture, the removal of DAYN is better than TIGY.

Characterization of the prepared adsorbents

SEM, EDX, and TEM analyses

The surface morphology, porosity, and microscopic features of SCBC and Ni-SCBC were examined using SEM, EDX, and TEM analyses. For SCBC, at various magnifications 5000×and 10,000×, SEM micrographs are shown in Fig. 3a, b, respectively. As could be observed, the surface looks comparatively smooth with the presence of carbon layers. Moreover, there are pores and cavities suggesting a high surface area and porosity. On the other hand, upon impregnation with NiO nanoparticles (Fig. 3c, d), the surface of Ni-SCBC becomes rough with many pits and holes, which in turn helps increase the surface area and positively affects the adsorption of TIGY and DAYN (Tejada-Tovar et al. 2021).

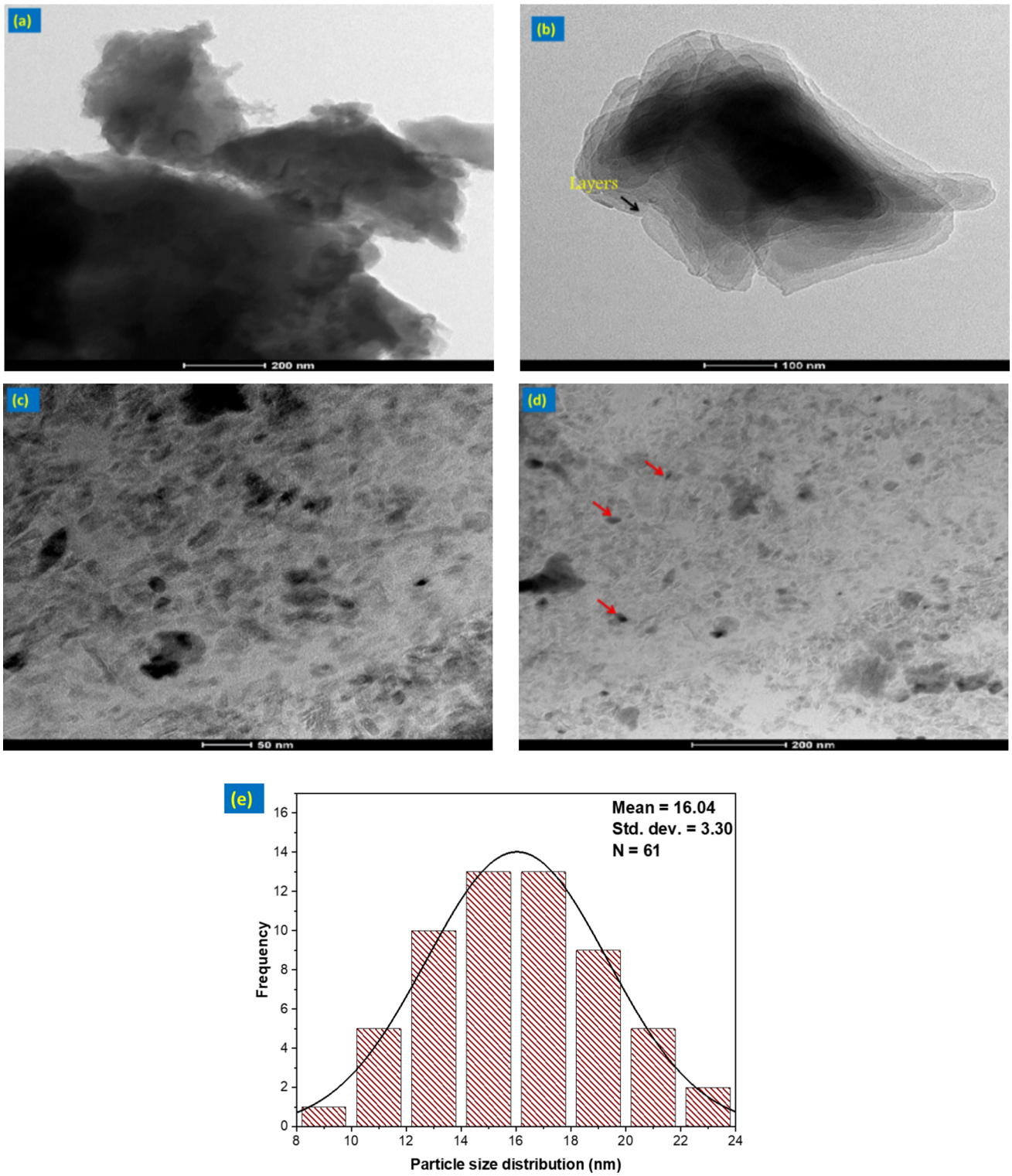

Fig. 4 TEM pictures of **a, b** SCBC, **c, d** Ni-SCBC, and **e** PSD of NiO nanoparticles in Ni-SCBC

EDX analysis is shown as inset tables in Fig. 3b, d. Analysis results indicated a considerable concentration of carbon (95.50%) and oxygen (4.50%) in the SCBC sample and confirmed the carbonaceous nature of the adsorbent following the treatment of the SC grounds thermally, justifying the removal efficiency of SCBC toward both drugs. On the other hand, a noticeable decrease of the % carbon (78.15%) in the case of Ni-SCBC, an increase in % oxygen

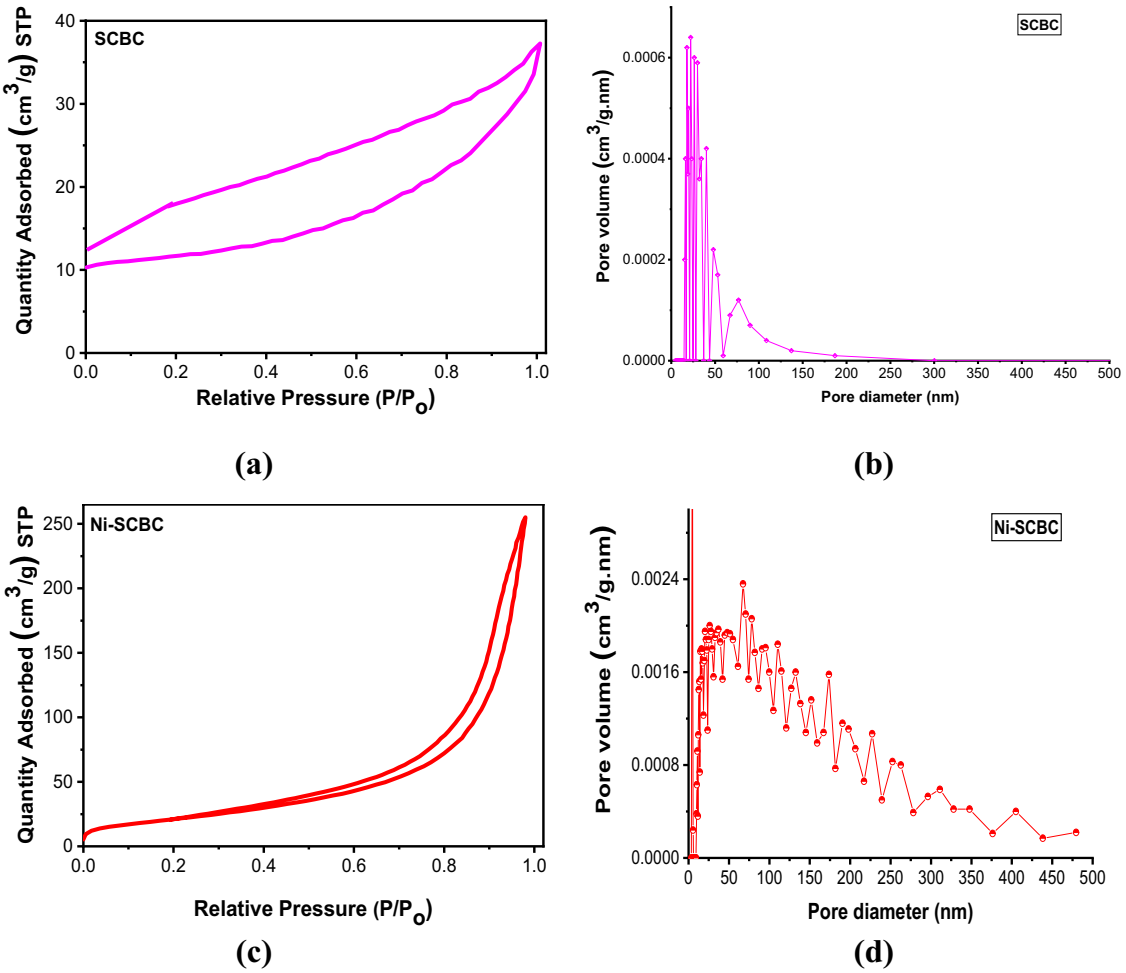

Fig. 5 N_2 adsorption–desorption isotherms and pore diameter for **a, b** SCBC, and **c, d** Ni-SCBC

(18.37%), and the appearance of Ni (3.48%) conform to the formation of NiO nanoparticles on the surface of the adsorbent, which also could explain the superior performance of Ni-SCBC compared to pristine biochar, SCBC. Further evidence of the successful loading of NiO nanoparticles on the surface of the biochar was quantitatively measured employing the inductively coupled plasma–optical emission spectrometry (ICP-OES). The amount of Ni (II) loaded on the biochar was found to be 6.30 ± 1.12 wt%, implying that more than 94% of Ni (II) was successfully loaded on the biochar surface.

Figure 4 shows the microstructural characterization of SCBC and Ni-SCBC using TEM analysis. The findings of the TEM analysis agreed well with the SEM micrographs. The SCBC surface is smooth and even with no particles on the surface (Fig. 4a, b). Conversely, the surface of the Ni-SCBC is rough, with NiO nanoparticles visible on the surface like tiny spheres (Fig. 4c, d). The average particle size of NiO nanoparticles was 16.04 ± 3.30 nm (Fig. 4e). A small particle size distribution (PSD) of 3.30 nm confirms the creation of uniform-sized NiO nanoparticles on the surface of the SCBC.

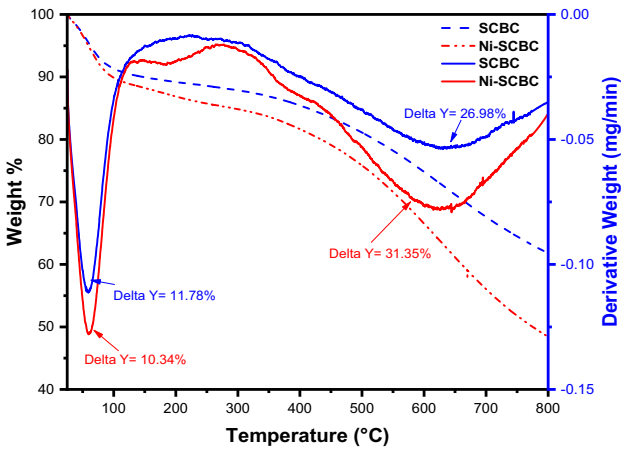

Fig. 6 TGA/*d*TA graphs of SCBC and Ni-SCBC

Analysis of surface area and pore size

Figure 5a–d reveals the N_2 adsorption/desorption isotherms as well as the pore volume of SCBC and Ni-SCBC. According to the results, the Langmuir surface area has increased from 49.23 m^2/g in SCBC to 86.06 m^2/g in the case of Ni-SCBC. This substantial increase in the surface area in the case of Ni-SCBC could be ascribed to the existence of NiO nanoparticles on the surface, which in turn positively affects the removal of DAYN and TIGY compared to the pristine biochar. Furthermore, SCBC and Ni-SCBC showed two types of pores based on the pore diameter: mesopores (2–50 nm) and macropores (˃ 50 nm). This mesoporous–macroporous structure enhances the drug uptake by the tested adsorbents. Moreover, the isotherm for both adsorbents was of type IV, suggesting monolayer and multilayer adsorption followed by capillary condensation. The hysteresis loop was of H3-type (Salunkhe et al. 2020), which is common in materials with a broad range of pore widths and indicate loose masses of platelike particles generating slit-like pores.

Thermal stability of the prepared adsorbents

TGA/*d*TA was used to assess the stability of both SCBC and Ni-SCBC under different temperatures (Fig. 6). In the case of Ni-SCBC, it could be observed that the %weight loss upon heating in the range of 50–350 °C was significant implying that the sample disintegrated entirely at 350 °C to produce NiO. The weight loss between 50 and 100 °C in the case of SCBC and Ni-SCBC was 11.78% and 10.34%, respectively, and could be ascribed to the evaporation of the physically adsorbed impurities and the thermal dehydration of $Ni(OH)_2$ in the case of Ni-SCBC (Deshpande et al. 2016). The results show that both samples are thermally stable in the temperature range of 350–450 °C. However, in the range of 550–800 °C, weight loss of 26.98% and 31.35% could be found in case of SCBC and Ni-SCBC, respectively. It could be observed that the weight loss of Ni-SCBC was higher than that of SCBC, between 550 and 800 °C. This behavior aligns with the previous studies (Du et al. 2019; Richardson et al. 2010; Silva et al. 2001) where nickel nitrate decomposes at high temperature to form HNO_3 and NO_x by-products. These compounds can oxidize SCBC biomass, producing CO and CO_2, leading to higher weight loss.

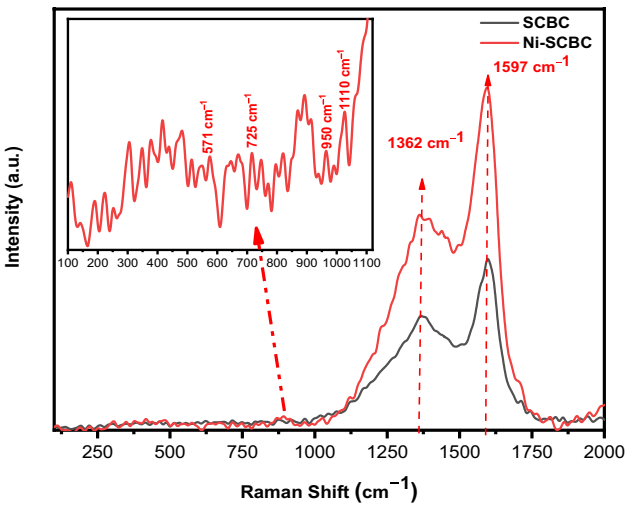

Fig. 7 Raman spectra for SCBC and Ni-SCBC

Raman spectroscopic analysis

Raman spectroscopy is commonly used to identify the vibrational modes of the studied molecules and to verify the rotational and other low-frequency modes of the studied systems (Adya and Canetta 2020). The Raman spectra of both adsorbents are shown in Fig. 7. At 1362 cm^{-1} (*D*-band) and 1597 cm^{-1} (*G*-band), two distinct bands that are commonly indicative of the formation of carbonaceous materials were spotted. For the sp^2 system, the *D*-band represents carbon lattice characteristics such as defects and sizes, whereas the *G*-band signifies the C–C stretching. The increase in the Raman intensity in case of Ni-SCBC confirms the successful loading of NiO nanoparticles on the surface. Additionally, the peaks between 400 and 1110 cm^{-1} elucidate the NiO spinel structure. The Raman mode of one-phonon (1P) first-order transverse TO, first-order longitudinal LO modes (at 571 cm^{-1}), two-phonon (2P) second-order transverse 2TO modes (at 725 cm^{-1}), and a mixture of TO + LO phonon excitation modes (at 950 cm^{-1}), and second-order longitudinal 2LO modes (at 1110 cm^{-1}) are illustrated in the inset spectrum. These excitation modes represent the vibration of Ni bonded to oxygen and confirm the presence of NiO on the surface (Mironova-Ulmane et al. 2007; Salunkhe et al. 2020). The presence of the NiO enhanced the removal of both TIGY and DAYN. This enhancement is attributed to the increase in the number of adsorption sites on the SCBC surface and possibly the formation of bonds between NiO and the two drugs.

Surface functionalities: FT-IR spectroscopic analysis

Functional groups on the surface of SCBC and Ni-SCBC were identified using FT-IR spectroscopic analysis (Fig. 8a). With slight variations in the peak positions, obtained results revealed that both SCBC and Ni-SCBC possess similar functionalities. The absence of an absorption peak at 3300 cm^{-1}

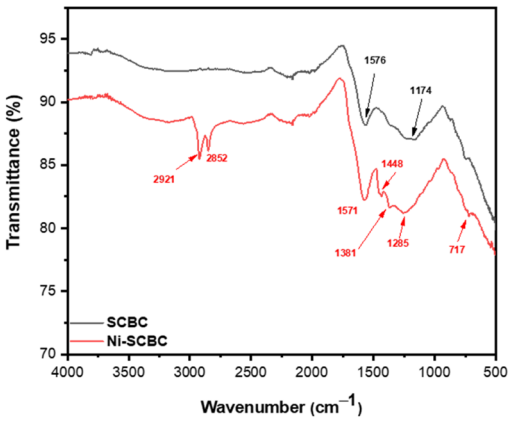
Transmittance (%)
Wavenumber (cm^{-1})
SCBC
Ni-SCBC
1576
1174
2921
2852
1448
1571
1381
1285
717

(a)

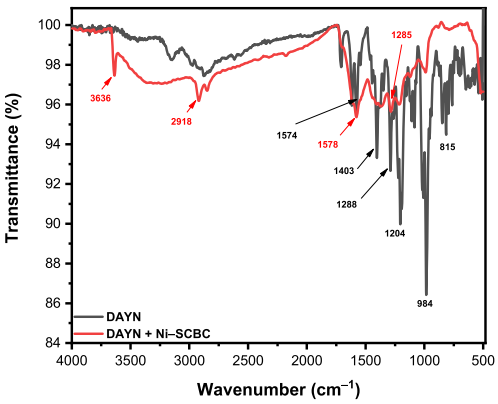
Transmittance (%)
Wavenumber (cm^{-1})
DAYN
DAYN + Ni–SCBC
3636
2918
1574
1578
1285
1403
1288
1204
984
815

(b)

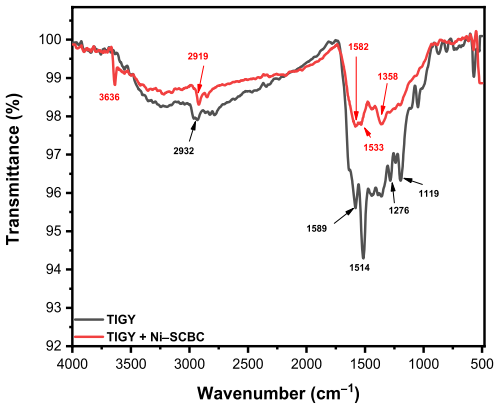
Transmittance (%)
Wavenumber (cm^{-1})
TIGY
TIGY + Ni–SCBC
3636
2919
2932
1582
1358
1533
1119
1276
1589
1514

(c)

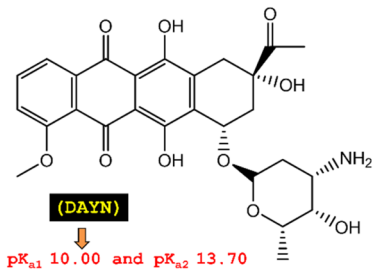
(DAYN)
pK$_{a1}$ 10.00 and pK$_{a2}$ 13.70

(d)

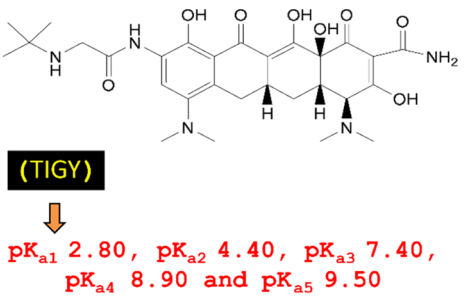
(TIGY)
pK$_{a1}$ 2.80, pK$_{a2}$ 4.40, pK$_{a3}$ 7.40,
pK$_{a4}$ 8.90 and pK$_{a5}$ 9.50

(e)

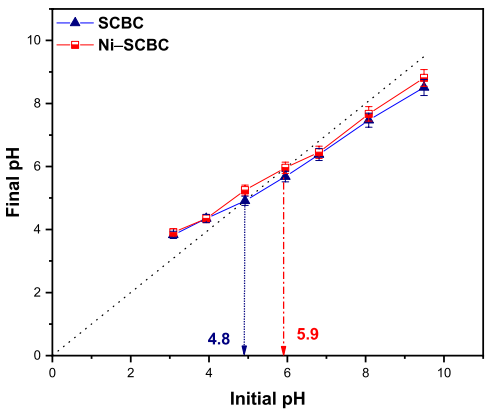
SCBC
Ni–SCBC
Final pH
Initial pH
4.8
5.9

(f)

◂**Fig. 8** FT-IR spectra of **a** SCBC and Ni-SCBC, **b, c** Ni-SCBC before and after adsorption of **b** DAYN and **c** TIGY, chemical structure with the pK_a values for **d** DAYN and **e** TIGY, **f** pH_{PZC} for both adsorbents

which is associated with hydrogen-bonded O – H from water in the spectra of both adsorbents indicates complete dehydration throughout the carbonization process (El-Azazy et al. 2022). Typical peaks can also be identified in the spectra of SCBC and Ni-SCBC. For instance, the peaks at 2921 cm^{-1} and 2852 cm^{-1} could be attributed to the aliphatic C – H and the C – C stretching vibrations for the alkyne. The peak at 1381 cm^{-1} represents the N – H stretching, at 1174 cm^{-1} is due to C – N stretching in SCBC, and other peaks such as 1448 cm^{-1} and 1285 cm^{-1} represent the alkene C – H bending. The presence of NiO nanoparticles on the surface was confirmed. This could be elucidated by the peak at 1576 cm^{-1} in SCBC and attributed to the carboxylic C = O and the aromatic C = C stretching, and this peak has slightly shifted to 1571 cm^{-1} in the Ni-SCBC because of the bond formation between NiO and the pristine SCBC (El-Azazy et al. 2021a; Sertoli et al. 2019). Another evidence of the presence of NiO nanoparticles on SCBC is the peak at 717 cm^{-1}, which could be assigned to the Ni – O stretching vibration (Baig et al. 2020; Sharma et al. 2014).

Figure 8b, c demonstrates the FT-IR spectra of DAYN and TIGY before and after adsorption onto Ni-SCBC. In Fig. 8b, the peaks between 815 cm^{-1} and 984 cm^{-1} correspond to the C = O and C – OH stretching vibrations of DAYN. The peaks at 1204 cm^{-1} and 1403 cm^{-1} represent the C – C = O bending vibrations and the aromatic C – H, respectively. The peaks at 1288 cm^{-1} and 1574 cm^{-1} attributed to the C – N stretching of the aromatic amine and the aromatic C = C stretching, respectively, were slightly shifted to 1285 cm^{-1} and 1578 cm^{-1} following the adsorption of DAYN, confirming the successful adsorption of DAYN onto Ni-SCBC (Kaczmarek et al. 2013; Lian and Meng 2017; Szafraniec et al. 2016). In Fig. 8c, the peaks between 1119 and 1276 cm^{-1} could be ascribed to the C – N and CH_3 stretching, respectively. The peaks at 1514 cm^{-1} and 3636 cm^{-1} represent the CH_3 bending vibrations. A slight shift in peaks of TIGY after adsorption onto Ni-SCBC was observed. For example, the peak at 1589 cm^{-1}, which is related to aromatic C – H bending, was shifted to 1582 cm^{-1}. Moreover, the peak at 2932 cm^{-1} that could be related to CH_3 stretching has shifted to 2919 cm^{-1}, confirming the adsorption of TIGY onto the Ni-SCBC (Menazea et al. 2020; Sabitha and Rajiv 2015; Trivedi et al. 2015). The changes and the shifts in the peak positions could be used to propose the adsorption mechanism together with the Box–Behnken design findings.

Proposed adsorption mechanism

Several mechanisms could be proposed to interpret the adsorption of DAYN and TIGY onto Ni-SCBC from their single and binary mixtures, including hydrogen bonding, electrostatic attraction, coordination interaction, intra-particle, and surface diffusion (Abdel-Hady et al. 2022). The structure of either drug (with several benzene or other aromatic rings) has electron-rich or electron-deficient groups that might cause interactions in aqueous solutions. Hydrogen bonding might take place between the nitrogen and oxygen atoms (H-acceptors) of the prepared adsorbents and the hydrogen of the hydroxyl groups (H-donors) of the drug molecule. Non-covalent π–π interactions between DAYN or TIGY aromatic rings and the aromatic backbone of the adsorbent is another mechanism (El-Azazy et al. 2021b). The same mechanism (π–π stacking, however, between the two drug molecules) could explain the decrease in adsorption from the binary mixture compared to the single solutions.

The electrostatic attraction mechanisms are often explained considering the interaction between the positively charged adsorbent and the negatively charged sites of the pollutant molecules (Fig. 8d–f). It is noteworthy to mention that the removal of DAYN and TIGY was negatively impacted by increasing the pH which could be further explained based on the analysis of the relationship between pH, pH_{PZC}, and pK_a of the target drugs. The pH_{PZC} for the prepared adsorbents, shown in Fig. 8f, demonstrated that SCBC had a pH_{PZC} of 4.8 ± 0.2 before being impregnated with NiO nanoparticles, compared to 5.9 ± 0.2, following the impregnation. These results are similar to the previously reported pH_{PZC} for SCBC (Franca et al. 2009; Lafi et al. 2014). As a result, the surface of the adsorbent might be positively charged at a pH value less than 4.8 ± 0.2 and 5.9 ± 0.2 for SCBC and Ni-SCBC, respectively. Therefore, at a pH value of 5.0 ± 0.2 (Box–Behnken design lower bound, and the optimum pH value as per the design analysis findings), the surface of the Ni-SCBC will be positively charged while that of SCBC is almost neutral. Occurrence of electrostatic interaction between the drug and the adsorbent is therefore more probable to occur with Ni-SCBC compared to SCBC, justifying the superior adsorption capacity of the former compared to the latter. The difference in the removal efficiency of Ni-SCBC toward DAYN and TIGY, could be related to the impact of their pK_a values (Fig. 8d, e). As shown, the pK_a of DAYN is 10.0 and 13.7, while TIGY has pK_a values of 2.8, 4.4, 7.4, 8.9, and 9.5 (El-Azazy et al. 2021a; Kiraly and Martin 1982). As such, DAYN will be therefore positively charged at the optimum pH value, suggesting that the electrostatic interaction between DAYN and

Table 6 Isotherm model equations

Isotherm models	Equations	Model parameters
Langmuir	$q_e = \frac{q_m K_L C_e}{1+K_L C_e}$ $R_L = \frac{1}{1+K_L C_0}$	q_m: Maximum adsorption capacity K_L: Langmuir equilibrium coefficient R_L: The DAYN and TIGY separation factor C_0 (mg/L): Initial concentration C_e (mg/L): Concentration at equilibrium
Freundlich	$q_e = K_F C_e^{\frac{1}{n}}$	K_F, $1/n$: Freundlich constants C_e (mg/L): Concentration at equilibrium
Temkin	$q_e = \frac{RT}{b_T}\ln(A_T C_e)$	R: The universal gas constant (8.314 J/mol.K) T: temperature (K) A_T, b_T: Temkin isotherm constants C_e (mg/L): Concentration at equilibrium
Dubinin–Radushkevich (D–R)	$q_e = q_s . \exp(-\beta.\epsilon^2)$ $\epsilon = RT\left(1+\frac{1}{C_e}\right)$ $E = 1/\sqrt{2\beta}$	q_s: Saturation capacity β: Activity coefficient ϵ: Calculated Polanyi potential E: Adsorption energy (kJ/mol)
Extended Langmuir isotherm (for binary mixture) model	$q_{e_{\mathrm{DAYN}}} = \frac{q_{m_{\mathrm{DAYN}}} K_{L_{\mathrm{DAYN}}} C_{e_{\mathrm{DAYN}}}}{1+K_{L_{\mathrm{DAYN}}} C_{e_{\mathrm{DAYN}}} + K_{L_{TIGY}} C_{e_{TIGY}}}$ $q_{eTIGY} = \frac{q_{m\_\mathrm{TIGY}} K_{L\_\mathrm{TIGY}} C_{e\_\mathrm{TIGY}}}{1+K_{L\_\mathrm{DAYN}} C_{e\_\mathrm{DAYN}} + K_{L\_\mathrm{TIGY}} C_{e\_\mathrm{TIGY}}}$	q_e: Adsorption capacity (mg/g) q_m: Maximum adsorption capacity K_L: Langmuir equilibrium coefficient C_e (mg/L): Concentration at equilibrium

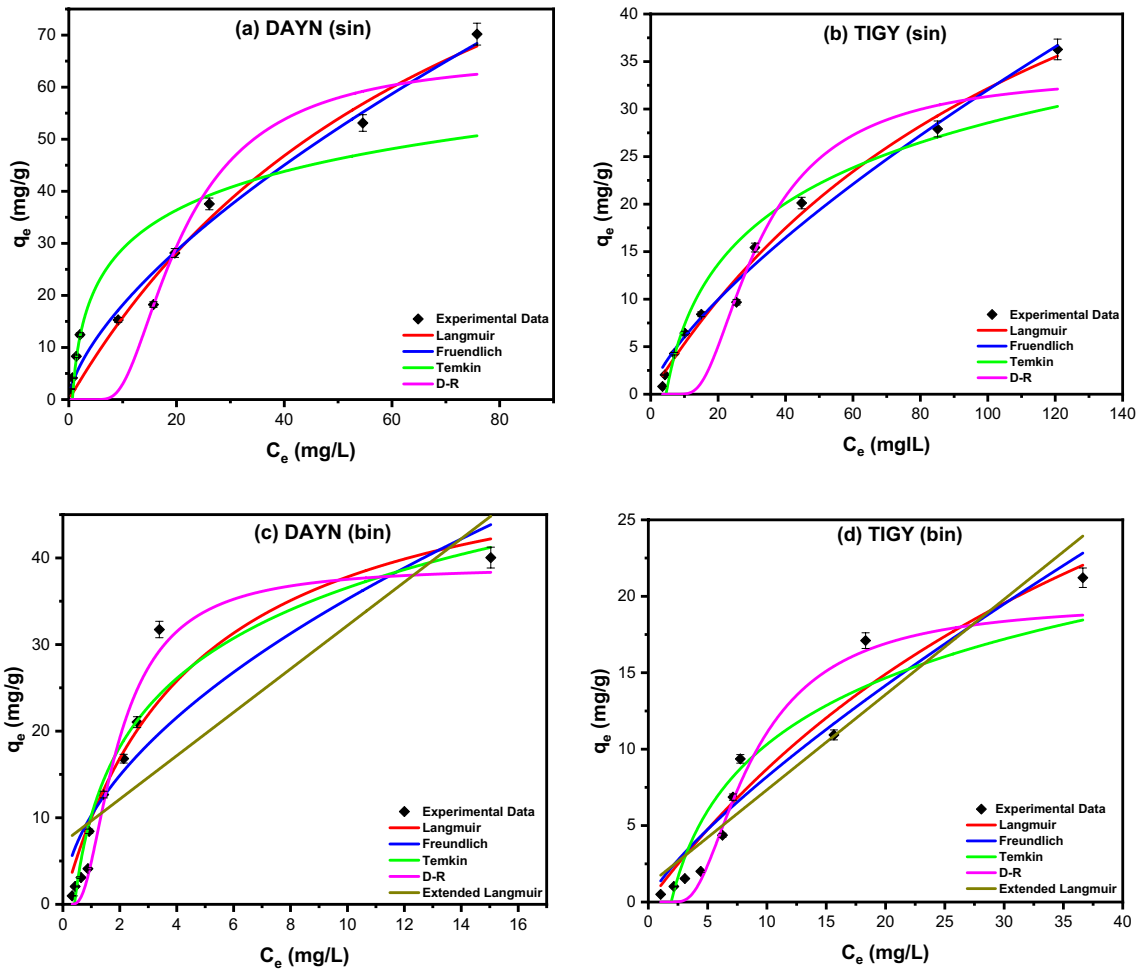

Fig. 9 Adsorption isotherms for the adsorption of TIGY and DAYN onto Ni-SCBC from **a, b** single solutions and **c, d** binary mixtures

the positively charged Ni-SCBC surface might not be the reason for DAYN uptake. In this case, the surface area of the adsorbent could rationalize the high uptake of DAYN via the formation of multilayers on the adsorbent's surface. On the other hand, the pK_a of TIGY shows an amphoteric state. Therefore, there is a probability of occurrence of repulsion between TIGY and the positively charged surface of Ni-SCBC adsorbent if pH is lower than the pK_a and the occurrence of electrostatic attraction if the pH is higher than the pK_a. In the latter case, formation of a monolayer of TIGY on the adsorbent's surface limits the uptake of TIGY.

Isotherm study

Most of the adsorption research is mainly focused on the removal of a single pollutant by various adsorbents. In contrast to this ideal situation, wastewater usually contains a mixture of pollutants. Another fact is that multi-component adsorption equilibrium modelling, which is critical in the design of a treatment system, is frequently overlooked. Therefore, it would be more realistic to look at the effects of binary combinations than to study the single-component systems. The existence of many drugs simultaneously is one of the most critical issues, and consequently, the interactions and competition between various drugs on the adsorption sites justify the need for further investigations. Adsorption equilibria that describe the competition between molecules on the adsorption sites are commonly utilized to better understand the behavior of the binary system components. As a result, many isotherms have been devised to represent equilibrium in such systems, such as the extended Langmuir isotherm model (Farajpourlar et al. 2013; Febrianto et al. 2009; Foo and Hameed 2010; Jebali et al. 2015).

Adsorption isotherms are usually applied to calculate the amount of adsorbate accumulated on the surface in addition to the adsorbent–adsorbate interactions. In this rehearsal, the adsorption of DAYN and TIGY from a single solution was investigated using four models: Langmuir, Freundlich,

Table 7 Calculated parameters for the adsorption equilibrium models used for the adsorption of both DAYN and TIGY onto Ni-SCBC nanosorbent from single solution (sin) and binary mixture (bin). Findings of the error functions' analysis are shown next to each model

Langmuir	q_m (mg/g)	K_L (L/mole)	RMSE (%)	ARE (%)	MAE (%)	MSE (%)	R^2
DAYN (sin)	136.62	0.013	4.20	2.62	3.40	17.64	0.9611
TIGY (sin)	73.15	0.008	1.22	1.54	1.00	1.48	0.9884
DAYN (bin)	54.85	0.222	3.55	6.39	2.75	12.61	0.9217
TIGY (bin)	51.84	0.021	1.73	4.88	1.56	3.00	0.9369
Freundlich	1/*n*	K_F (mole/g) (L/mole)$^{1/n}$	RMSE (%)	ARE (%)	MAE (%)	MSE (%)	R^2
DAYN (sin)	0.65	4.026	3.36	0.74	2.66	11.27	0.9758
TIGY (sin)	0.73	1.132	1.42	3.19	1.23	2.03	0.9845
DAYN (bin)	0.54	10.27	5.23	9.39	4.25	27.39	0.8302
TIGY (bin)	0.79	1.335	1.96	5.29	1.72	3.83	0.9172
Temkin	b_T (J/mole)	A_T (L/mole)	RMSE (%)	ARE (%)	MAE (%)	MSE (%)	R^2
DAYN (sin)	231.12	1.489	9.81	84.28	7.61	453.7	0.7881
TIGY (sin)	268.24	0.219	3.27	20.21	2.62	124.01	0.9138
DAYN (bin)	216.74	2.449	3.26	5.64	2.57	161.11	0.9339
TIGY (bin)	395.42	0.518	2.53	9.25	2.22	46.25	0.8619
D–R	β	E (kJ/mole)	q_m (mg/g)	RMSE (%)	ARE (%)	MAE (%)	MSE (%)	R^2
DAYN (sin)	1.11×10^{-7}	3.00	66.25	34.31	38.67	31.69	1177	0.8815
TIGY (sin)	2.61×10^{-7}	1.96	33.90	8.71	13.82	7.82	75.82	0.8806
DAYN (bin)	1.40×10^{-8}	8.45	39.02	13.26	35.24	12.02	175.71	0.9559
TIGY (bin)	2.05×10^{-8}	6.98	19.65	5.63	21.59	5.04	31.69	0.9285
Extended Langmuir	q_m (mg/g)	K_{L_DAYN} (L/mole)	K_{L_TIGY} (L/mole)	RMSE (%)	ARE (%)	MAE (%)	MSE (%)	R^2
DAYN (bin)	58.42	1.746	0.059	6.01	12.68	6.84	34.03	0.6862
TIGY (bin)	23.50	0.015	0.807	9.68	33.37	8.13	93.77	0.8886

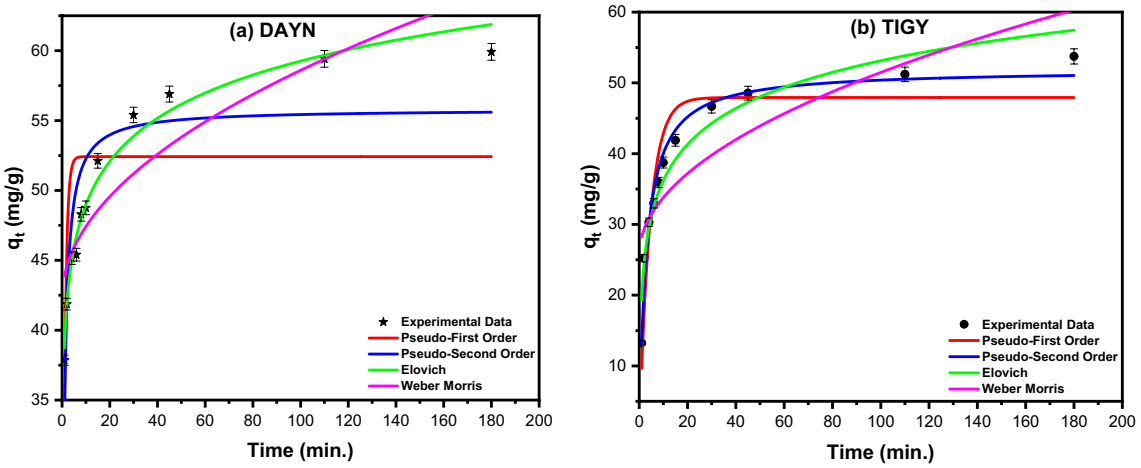

Fig. 10 Kinetic models for the adsorption of **a** DAYN and **b** TIGY onto Ni-SCBC

Temkin, and Dubinin–Radushkevich (D–R) (Dubinin 1947; Freundlich 1907; Langmuir 1918; Temkin 1940) (Table 6). These four models were utilized, together with the extended Langmuir isotherm, to investigate the adsorption of DAYN and TIGY from their binary mixture (El-Azazy et al. 2023).

Statistical error indices were employed to evaluate the accuracy of the studied isotherms. Employed functions

Table 8 Calculated parameters for the four kinetic models used to investigate the adsorption of DAYN and TIGY onto Ni-SCBC. Findings of the analysis of the error functions are shown following each model

Model and equation	Parameter	Parameter definition	Value	
			DAYN	TIGY
Pseudo-first order (PFO) $\frac{dq_t}{dt} = k_1(q_e - q_t)$	K_1 (1/min)	K_1: Adsorption rate constant	1.027	0.225
	q_e (mg/g)	q_t: capacity at time t	52.42	47.93
	RMSE (%)		5.10	4.09
	ARE (%)		0.07	0.40
	MAE (%)		4.67	3.58
	MSE (%)		25.96	16.71
	R^2		0.4622	0.8766
Pseudo-second order (PSO) $\frac{dq_t}{dt} = k_2(q_e - q_t)^2$	K_2 (g/(mg.min))	K_2: Adsorption rate constant	0.026	0.006
	q_e (mg/g)	q_t: capacity at time t	55.81	51.88
	RMSE (%)		3.20	1.97
	ARE (%)		0.01	0.31
	MAE (%)		2.83	1.36
	MSE (%)		10.25	3.88
	R^2		0.7878	0.9748
Elovich model $q_t = \frac{1}{\beta} \times ln(1 + \alpha\beta t)$	α	α, β: Elovich constants	26,324	101.69
	β		0.224	0.136
	RMSE (%)		1.05	2.73
	ARE (%)		0.02	0.27
	MAE (%)		0.84	2.24
	MSE (%)		1.10	7.44
	R^2		0.9773	0.9451
Weber – Morris model (WM) $q_t = K_I t^{0.5} + C$	K_1	K_I: Intra-particle diffusion rate constant	1.64	2.58
	C	C: Thickness of the boundary layer	42.24	25.63
	RMSE (%)		3.17	6.31
	ARE (%)		0.06	0.80
	MAE (%)		2.58	5.02
	MSE (%)		10.02	39.87
	R^2		0.7924	0.7057

included the root mean square error (RMSE), average relative error (ARE), mean absolute error (MAE), and mean square error (MSE) (Table S2). The RMSE was used to evaluate the average adsorption capacity of the collected data from the fitted regression nonlinear equation. In addition, the ARE and MAE error values were used to assess the variance between the predicted adsorption capacity and the observed values. The MSE was used to estimate the average square difference between the predicted adsorption capacity and the observed responses.

Applying the Langmuir isotherm model, the following assumptions could be comprehended: (I) all adsorption sites on the Ni-SCBC surface are equivalent, (II) no interaction between the adsorbed species, and (III) adsorption results in the formation of a uni-molecular layer. The Langmuir isotherm model is depicted in Fig. 9a, b for the individual drug solutions, and Fig. 9c, d for their binary mixture. The value of the separation factor, R_L, can establish the type of adsorption. In the current approach, the value of R_L was < 1, suggesting that the process was favorable. Furthermore, at higher drug concentrations, the adsorption became irreversible, with a q_m value of 136.62 and 73.15 mg/g for DAYN and TIGY in their single solutions, respectively. The q_m value in the binary mixture, on the other hand, was reduced to 54.85 mg/g for DAYN and 51.84 mg/g for TIGY (Table 7), which could be attributed to the competition between the two drugs on the adsorption sites. The obtained results conform to the findings of the Box–Behnken design.

Values of the Freundlich model parameters are displayed in Table 7. The data collected for single drug solutions (Fig. 9a, b) demonstrate that the adsorption of DAYN(sin) matches well with the Freundlich isotherm. This could be comprehended from the highest R^2-value (0.9758) and the lowest RMSE%, ARE%, MAE%, and MSE% error values compared to the other models. Adsorption of TIGY(sin), however, matches the Langmuir isotherm (highest R^2-value

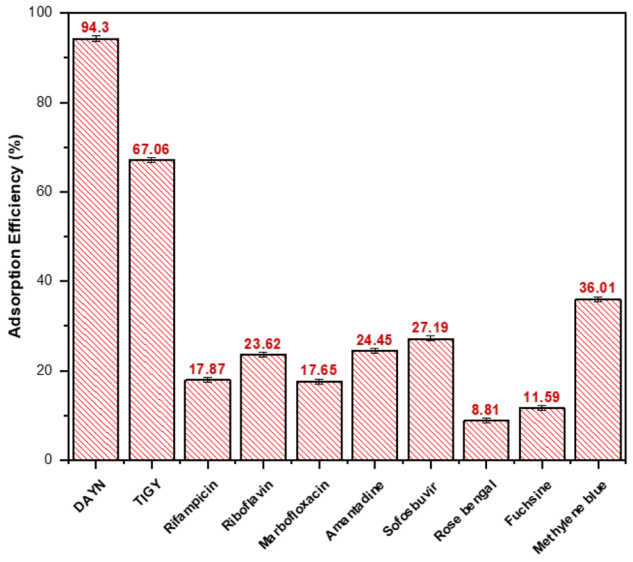

Fig. 11 Adsorption selectivity of Ni-SCBC toward DAYN and TIGY compared to different drugs and dyes. The measurements were taken in triplicate, and the results were presented as the mean value ± SD

of 0.9884 and lowest error values). The DAYN(sin) has a $1/n = 0.65$, $n = 1.54$, while the TIGY (sin) has a $1/n = 0.73$, $n = 1.37$. Therefore, the adsorption potential for DAYN(sin) will be higher compared to TIGY(sin). Furthermore, the obtained data for both DAYN and TIGY in the binary mixture fitted well to the Langmuir isotherm, as confirmed by lowest error and highest R^2 (0.9217 and 0.9369 for DAYN(bin) and TIGY(bin), respectively).

Temkin isotherm is used to depict the adsorbate–adsorbent interactions. DAYN(sin) has an adsorption energy of 231.12 J/mol, while TIGY(sin) has an adsorption energy of 268.24 J/mol, as shown in Fig. 9a–d and Table 7. These results show that DAYN and TIGY are effectively adsorbed onto the surface of the Ni-SCBC nanosorbent from their single solution and agree with the Langmuir and Freundlich models' findings. The same conclusions were obtained for the binary mixture, with adsorption energies of 216.74 and 395.42 J/mol for DAYN and TIGY, respectively.

Dubinin–Radushkevich (D–R) model was utilized to find out the adsorption mechanisms of both drugs onto Ni-SCBC (Fig. 9a–d, Table 7). The obtained results indicated that the adsorption energy of DAYN(sin) is 3.00 kJ/mol compared to 1.96 kJ/mol in the case of TIGY(sin), implying that the adsorption of both drugs from their single solutions is physisorption with sorption energy < 8 kJ/mol. The physisorption mechanism could be mainly related to the higher surface area of Ni-SCBC as confirmed by the surface area and pore size analysis findings. The binary mixture data, however, showed a different pattern, with adsorption energies of 8.45 and 6.98 kJ/mol for DAYN(bin) and TIGY(bin), respectively, suggesting chemisorption in the case of DAYN and physisorption for TIGY from their binary mixture.

The adsorption of a DAYN and TIGY in their binary mixture solutions was studied using the extended Langmuir isotherm model (Table 7). The obtained data show that R^2-values for DAYN(bin) and TIGY(bin) are 0.6862 and 0.8886, respectively, which are quite low compared to the previous isotherms. These data were also confirmed by the error function values (Table 7). Therefore, the extended Langmuir isotherm might not be sufficient to describe the adsorption equilibrium of both drugs onto Ni-SCBC in a binary system. Table 7 shows that the q_m value of Ni-SCBC in a multi-component solution was reduced for both drugs, 58.42 and 23.50 mg/g, for DAYN and TIGY, respectively.

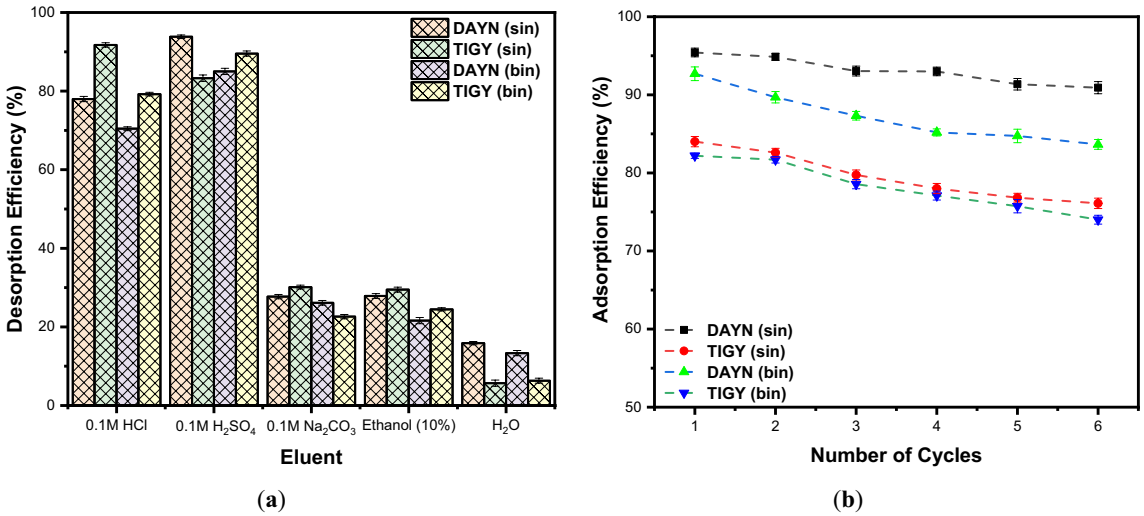

Fig. 12 **a** Effect of different eluents on desorption of both DAYN and TIGY from single and binary mixtures from Ni-SCBC**,** and **b** regeneration studies of the studied adsorbent Ni-SCBC toward the removal of both DAYN and TIGY from single and binary mixture

Obtained data, therefore, confirm the competition of both drugs for the active sorption sites as reflected by reduced q_m values (Issa et al. 2014).

Kinetic models

Four kinetic models were used to investigate the adsorption of DAYN and TIGY onto Ni-SCBC: pseudo-first-order (PFO), pseudo-second-order (PSO), Elovich, and Weber–Morris (WM) (Ho and McKay 1999; Lagergren 1898; Weber and Morris 1963; Wu et al. 2009) (Fig. 10a, b). Table 8 displays the estimated parameters for the examined models. According to the findings, the R^2 -value for the PSO model is in a good match for the adsorption of both drugs onto Ni-SCBC (0.7878 and 0.9748, respectively). The obtained data can be further confirmed by the low value of the error functions. Based on these findings, the drug and the adsorbent concentrations control the rate of the adsorption interaction between both TIGY, DAYN, and the Ni-SCBC nanosorbent.

In general, the PFO and PSO are not capable of outlining the diffusion mechanisms. On the other hand, as per Elovich model, the rate of drug adsorption initially rises quickly but eventually it reaches a maximum point when the available surface area becomes saturated with the adsorbed molecules. This model also provides the Elovich constant, which is associated with the activation energy of the adsorption process, and it can be used to measure the strength of the interaction between the drug molecules and the Ni-SCBC surface. Obtained data show that DAYN adsorption conforms well to the Elovich model (as well as the PSO model), with the highest R^2 value of 0.9773 and the lowest RMSE, ARE, MAE, and MSE % error (1.05%, 0.02%, 0.84%, and 1.10%, respectively). Furthermore, the initial adsorption rate of DAYN was obtained using the Elovich model. The initial adsorption rate in case of DAYN was much higher, 26,324 mg/(g min), compared to TIGY (101.69 (mg/g min)).

Finally, compared to the other kinetic models, the R^2-value of WM model was too low, and the error was very high for both drugs, and it could not be utilized to explain their adsorption onto the Ni-SCBC nanosorbent.

Adsorption selectivity of Ni-SCBC

To test the adsorbent selectivity, the adsorption efficiency of Ni-SCBC toward DAYN and TIGY was compared to that of eight other drugs and dyes with varying chemical structures and pharmacological properties. Figure 11 shows that Ni-SCBC exhibited a significant adsorption efficiency of 94.30% and 67.06% toward DAYN and TIGY, respectively. Conversely, the adsorption efficiency for the other drugs and dyes was relatively lower compared to that of DAYN and TIGY. The adsorption efficiency toward the tested compounds was between 8.81% and up to 36.01%, indicating a low affinity of Ni-SCBC toward these compounds. This can be attributed to several factors, such as the effectiveness of the factorial blend used during adsorption for each pollutant, the relationship between the adsorbent's pH_{PZC} and the adsorbate's pK_a, and the chemical structure of the pollutant. The highest pollutant uptake was observed for methylene blue, with a $\%R$ of 36.01%. Notably, the pK_a of methylene blue is 3.8 (Sen 2023). Since the pH_{PZC} of the adsorbent Ni-SCBC is 5.9, the surface becomes positively charged at pH 5. Therefore, methylene blue carries a negative charge, resulting in an effective interaction with the surface and subsequent removal of the dye. On the other hand, rifampicin showed a lower $\%R$ of 17.87% as a result of the difference between the pH_{PZC} and the pK_a of the drug, which is 1.7 and 7.9, respectively (Howes et al. 2007). These pK_a values suggest a zwitterionic structure, which negatively affects the removal efficiency at pH 5.

Desorption and Ni-SCBC recovery studies

The economic applicability of any adsorbent is crucial, and it is mostly determined by adsorbent regeneration. A desorption investigation study was conducted for this purpose using five distinct eluents, followed by six sequential adsorption–desorption cycles. Five eluents were evaluated for the desorption of both DAYN and TIGY from loaded Ni-SCBC, including 0.1 M solutions of hydrochloric acid, sulfuric acid, and sodium carbonate, in addition to 10% ethanol and water. Figure 12a depicts the relationship between the tested eluents and the desorption efficiency (%). The obtained data for the single solution revealed that 0.1 M sulfuric acid was the best eluent for DAYN, compared to 0.1 M hydrochloric acid in case of TIGY, with desorption efficiency of 93.97% and 91.63%, respectively. In case of the binary mixture, the optimal eluent was 0.1 M sulfuric acid for both drugs, with a desorption efficiency of 84.59% and 83.29% for DAYN and TIGY, respectively. As a result, 0.1 M sulfuric and hydrochloric acids were chosen as the best eluents for desorbing DAYN and TIGY from loaded Ni-SCBC.

Cyclic adsorption–desorption studies were carried out for the adsorbent regeneration studies, and the results are presented in Fig. 12b. The acquired findings show that DAYN removal effectiveness from both single solution and binary mixture using Ni-SCBC adsorbent was decreased slightly from 95.42% (cycle 1) to 90.91% (cycle 6) for a single solution and decreased from 92.70% (cycle 1) to 83.65% (cycle 6). Besides, the same results were also obtained for the TIGY single solution and primary mixture. These data

demonstrate that the investigated adsorbent is stable and can be effectively regenerated and utilized for more than six cycles with more than 80% removal effectiveness.

Cost analysis of the prepared adsorbents

To assess the economic feasibility of the prepared adsorbents, it is essential to consider the cost of all chemicals as well as the energy used. Compared to commercial adsorbents, food wastes (spent coffee grounds in this case) are available at no cost. Additionally, converting waste materials into value-added products can reduce the burden on the environment by properly recycling and reusing the waste (Ahmed et al. 2016). The estimated energy consumption for producing 1 kg of SCBC is 175.65 KWh/kg with an electricity tariff of 0.168 $/KWh (as of 2023, Qatar), which includes energy consumed by the oven and furnace. The total cost per kg of the SCBC is therefore 15.28 $. The reagents used in preparing 11 g of Ni-SCBC were oleylamine, *n*-propanol, $Ni(NO_3)_2{\cdot}6H_2O$, and ammonia solution, with a cost of 0.168 $, 1.015 $, 4.05 $, and 0.207 $, respectively. Therefore, the whole cost per g of Ni-SCBC is 0.556 $. Despite the higher cost of producing nickel-loaded biochar compared to the pristine SCBC, the higher adsorption capacity of Ni-SCBC should be considered.

Conclusions

This study aimed to remove two antibiotics, TIGY and DAYN, from synthetic wastewater samples. In this regard, two adsorbents were successfully produced using a readily abundant waste material: spent coffee grounds. A comparison between the performances of the pristine biochar (SCBC) and the nickel (II) oxide-impregnated candidate (Ni-SCBC) was convened. Ni-SCBC performed better toward both TIGY and DAYN, either from the single solutions or the binary mixture. To structure a green and sustainable, Box–Behnken design was operated to exert control over the variables impacting the adsorption process. In the same itinerary, the composite desirability function was used to decide upon the variables that could achieve the highest uptake of both DAYN and TIGY, simultaneously. Pareto charts confirmed that pH and [Drug] are the most significant variables. The highest removal efficiency of DAYN and TIGY from their single solutions was 94.30% and 67.06%, respectively. Comprehending the adsorbent behavior was attempted using different characterization techniques. The TGA/*d*TA analysis confirmed the thermal stability of both adsorbents in the range of 350–450 °C. FT-IR analysis obtained before and after impregnation with NiO revealed a shift in some peaks and the appearance of new peaks, confirming the presence of NiO nanoparticles. BET analysis showed that NiO impregnation increased the surface area (86.06 m^2/g) of the prepared nanosorbent. Nonlinear equilibrium studies revealed that DAYN(sin) adsorption fits well with the Freundlich isotherm, while TIGY(sin) matches the Langmuir model. On the other hand, Langmuir isotherm was of choice for both drugs in their binary mixture. Kinetic studies indicated that the PSO model better described the adsorption of both TIGY and DAYN onto Ni-SCBC. Selectivity of Ni-SCBC toward DAYN and TIGY was substantiated versus an array of other potential pollutants. Reusability of Ni-SCBC was confirmed for more than 6 cycles with more than 80% removal effectiveness.

The results of our investigation can be summed up as critical, hopeful, and novel. Our findings suggest that SCBC and Ni-SCBC could be used as effective and affordable adsorbents for the remediation of drug residues. For the elimination of organic contaminants in wastewater, carbon-based materials hold out a great deal of promise. The transition from the lab scale to the industry, more research must be done on SCBC and Ni-SCBC for drug reside removal, as determined in this work.

Supplementary Information The online version contains supplementary material available at https://doi.org/10.1007/s13201-024-02238-8.

Acknowledgements The project members would like to extend their special thanks to the Central Lab Unit (CLU) at Qatar University. The authors would also like to extend their gratitude to the laboratory members of Prof. Siham Alqaradawi's research group for accomplishing the BET analysis.

Funding This research was funded by Qatar University—Internal Student Grant 'QUST-1-CAS-2022–338.' All findings reported herein are the responsibility of the authors.

Data availability statement The data presented in this study are available within this article. Further inquiries could be directed to the authors.

Declarations

Conflicts of interest The authors declare no conflict of interest.

Ethical approval and consent to participate This article does not contain any studies with animals and human subjects. The authors confirm that all the study meets ethical guidelines and adheres to the legal requirements of the study country.

References

Abdel-Hady EE, Mahmoud R, Hafez SHM, Mohamed HFM (2022) Hierarchical ternary ZnCoFe layered double hydroxide as efficient adsorbent and catalyst for methanol electrooxidation. J Mater Res Technol 17:1922–1941. https://doi.org/10.1016/j.jmrt.2022.01.042

Adya AK, Canetta E (2020) Chapter 16: nanotechnology and its applications to animal biotechnology. In: Verma AS, Singh A (eds) Animal biotechnology, 2nd edn, pp. 309–326. Academic Press. https://doi.org/10.1016/B978-0-12-811710-1.00014-8

Ahmed MB, Zhou JL, Ngo HH, Guo W (2016) Insight into biochar properties and its cost analysis. Biomass Bioenergy 84:76–86. https://doi.org/10.1016/j.biombioe.2015.11.002

Almufarij RS, Abdulkhair BY, Salih M, Alhamdan NM (2022) Sweep-out of tigecycline, chlortetracycline, oxytetracycline, and doxycycline from water by carbon nanoparticles derived from tissue waste. Nanomater 12(20):3617. https://www.mdpi.com/2079-4991/12/20/3617

Babic MB, Milovijic SK, Polovina MJ, Kaludierovic BV (1999) Point of zero charge and intrinsic equilibrium constants of activated carbon cloth. Carbon 37:477–481. https://doi.org/10.1016/s0008-6223(98)00216-4

Baig U, Khan A, Gondal MA, Dastageer MA, Falath WS (2020) Laser induced anchoring of nickel oxide nanoparticles on polymeric graphitic carbon nitride sheets using pulsed laser ablation for efficient water splitting under visible light. Nanomater 10(6):1098. https://doi.org/10.3390/nano10061098

Basak BB, Sarkar B, Saha A, Sarkar A, Mandal S, Biswas JK, Wang H, Bolan NS (2022) Revamping highly weathered soils in the tropics with biochar application: What we know and what is needed. Sci Total Environ 822:153461. https://doi.org/10.1016/j.scitotenv.2022.153461

Basheer AA (2018) New generation nano-adsorbents for the removal of emerging contaminants in water. J Mol Liq 261:583–593. https://doi.org/10.1016/j.molliq.2018.04.021

Box GEP, Cox DR (1964) An analysis of transformations. J R Stat Soc Series B Stat Methodol 26(2):211–252. http://www.jstor.org/stable/2984418

Box GEP, Behnken DW (1960) Some new three level designs for the study of quantitative variables. Technometrics 2(4):455–475. https://doi.org/10.2307/1266454

Brel VK, Moiseeva AA, Artyushin OI, Anikina LV, Klemenkova ZS (2021) Simple methods of modification of daunorubicin on the daunosamine nitrogen atom. Med Chem Res 30(3):564–573. https://doi.org/10.1007/s00044-020-02664-8

Bumajdad A, Zaki MI, Eastoe J, Pasupulety L (2004) Microemulsion-based synthesis of CeO_2 powders with high surface area and high-temperature stabilities. Langmuir 20(25):11223–11233. https://doi.org/10.1021/la040079b

Cantarella M, Carroccio SC, Dattilo S, Avolio R, Castaldo R, Puglisi C, Privitera V (2019) Molecularly imprinted polymer for selective adsorption of diclofenac from contaminated water. J Chem Eng 367:180–188. https://doi.org/10.1016/j.cej.2019.02.146

Daghrir R, Drogui P (2013) Tetracycline antibiotics in the environment: a review. Environ Chem Lett 11(3):209–227. https://doi.org/10.1007/s10311-013-0404-8

Deshpande MP, Patel KN, Gujarati VP, Patel K, Chaki SH (2016) Structural, thermal and optical properties of nickel oxide (NiO) nanoparticles synthesized by chemical precipitation method. Adv Mat Res 1141:65–71. https://doi.org/10.4028/www.scientific.net/AMR.1141.65

do Amaral DF, Montalvão MF, de Oliveira Mendes B, da Costa Araújo AP, de Lima Rodrigues AS, Malafaia G (2019) Sublethal effects induced by a mixture of different pharmaceutical drugs in predicted environmentally relevant concentrations on *Lithobates catesbeianus* (*Shaw*, 1802) (*Anura, ranidae*) tadpoles. Environ Sci Pollut Res 26(1):600–616. https://doi.org/10.1007/s11356-018-3656-9

Dong Z, Abbas MN, Kausar S, Yang J, Li L, Tan L, Cui H (2019) Biological functions and molecular mechanisms of antibiotic tigecycline in the treatment of cancers. Int J Mol Sci 20(14):3577. https://doi.org/10.3390/ijms20143577

Du Z-Y, Zhang Z-H, Xu C, Wang X-B, Li W-Y (2019) Low-Temperature steam reforming of toluene and biomass tar over biochar-supported Ni nanoparticles. ACS Sustainable Chem Eng 7(3):3111–3119. https://doi.org/10.1021/acssuschemeng.8b04872

Dubinin MM (1947) The equation of the characteristic curve of activated charcoal. Dokl Akad Nauk SSSR 55:327–329

El-Azazy M, El-Shafie AS, Fawzy S, Rooney DW, Osman AI (2023) Competitive adsorptive removal of promazine and promethazine from wastewater using olive tree pruning biochar: operational parameters, kinetics, and equilibrium investigations. Environ Sci Pollut Res 30:82387–82405. https://doi.org/10.1007/s11356-023-27688-6

El-Azazy M, El-Shafie AS, Al-Meer S, Al-Saad KA (2021a) Eco-structured adsorptive removal of tigecycline from wastewater: date pits' biochar versus the magnetic biochar. Nanomater 11(1):30. https://www.mdpi.com/2079-4991/11/1/30

El-Azazy M, El-Shafie AS, Al-Shaikh Yousef B (2021b) Green tea waste as an efficient adsorbent for methylene blue: Structuring of a novel adsorbent using full factorial design. Molecules 26(20):6138. https://www.mdpi.com/1420-3049/26/20/6138

El-Azazy M, El-Shafie AS, Al-Saad KA (2022) Application of infrared spectroscopy in the characterization of lignocellulosic biomasses utilized in wastewater treatment. In El-Azazy M, El-Shafie AS, Al-Saad KA (eds), Infrared Spectroscopy: perspectives and applications pp. Ch. 8. IntechOpen. https://doi.org/10.5772/intechopen.108878

El-Shafie AS, Ahsan I, Radhwani M, Al-Khangi MA, El-Azazy M (2022) Synthesis and application of Cobalt Oxide (Co_3O_4)-Impregnated olive stones biochar for the removal of Rifampicin and Tigecycline: Multivariate controlled performance. Nanomater 12(3):379. https://www.mdpi.com/2079-4991/12/3/379

El-Shafie AS, Rahman E, GadelHak Y, Mahmoud R, El-Azazy M (2024) Techno-economic assessment of waste mandarin biochar as a green adsorbent for binary dye wastewater effluents of methylene blue and basic fuchsin: Lab- and large-scale investigations. Spectrochim Acta A Mol Biomol Spectrosc 306:123621. https://doi.org/10.1016/j.saa.2023.123621

Farajpourlar M, Ram S, Rao M, Rao VVB (2013) Studies on fixed and fluidized bed ion exchange column to treat wastewater. IOSR J Environ Sci Toxicol Food Technol 6:01–06

FDA (2017) FDA drug safety communication: Increased risk of death with Tygacil (tigecycline) compared to other antibiotics used to treat similar infections https://www.fda.gov/drugs/drug-safety-and-availability/fda-drug-safety-communication-increased-risk-death-tygacil-tigecycline-compared-other-antibiotics. Accessed 25 March 2023

Febrianto J, Kosasih AN, Sunarso J, Ju YH, Indraswati N, Ismadji S (2009) Equilibrium and kinetic studies in adsorption of heavy metals using biosorbent: a summary of recent studies. J Hazard Mater 162(2):616–645. https://doi.org/10.1016/j.jhazmat.2008.06.042

Foo KY, Hameed BH (2010) Insights into the modeling of adsorption isotherm systems. Chem Eng J 156(1):2–10. https://doi.org/10.1016/j.cej.2009.09.013

Franca AS, Oliveira LS, Ferreira ME (2009) Kinetics and equilibrium studies of Methylene Blue adsorption by spent coffee grounds. Desalination 249(1):267–272. https://doi.org/10.1016/j.desal.2008.11.017

Freundlich H (1907) Ueber die adsorption in loesungen. Z Phys Chem 57:385–470

Ghodrati A, Shahrouzi JR, Nemati R, Pourjafari N (2022) Adsorptive removal of Daunorubicin from water by graphene oxide, activated carbon, and multiwalled carbon nanotubes: equilibrium and kinetic studies. Chem Eng Technol 45(12):2203–2210. https://doi.org/10.1002/ceat.202200326

Globenewswire (2022) Global doxorubicin market research report (2021 to 2027) - by drug formulation, application, distribution channel and region. Retrieved 21-12-2022 from https://www.globenewswire.com/en/news-release/2022/02/02/2377673/28124/en/Global-Doxorubicin-Market-Research-Report-2021-to-2027-by-Drug-Formulation-Application-Distribution-Channel-and-Region.html. Accessed 30 March 2023

Gouveia TIA, Alves A, Santos MSF (2019) New insights on cytostatic drug risk assessment in aquatic environments based on measured concentrations in surface waters. Environ Int 133:105236. https://doi.org/10.1016/j.envint.2019.105236

Ho YS, McKay G (1999) Pseudo-second order model for sorption processes. Process Biochem 34:451–465

Howes BD, Guerrini L, Sanchez-Cortes S, Marzocchi MP, Garcia-Ramos JV, Smulevich G (2007) The influence of pH and anions on the adsorption mechanism of rifampicin on silver colloids. J Raman Spectrosc 38(7):859–864. https://doi.org/10.1002/jrs.1727

Issa AA, Al-Degs YS, Al-Ghouti MA, Olimat AAM (2014) Studying competitive sorption behavior of Methylene Blue and Malachite Green using multivariate calibration. Chem Eng J 240:554–564. https://doi.org/10.1016/j.cej.2013.10.084

Jebali A, Behzadi A, Rezapor I, Jasemizad T, Hekmatimoghaddam SH, Halvani GH, Sedighi N (2015) Adsorption of humic acid by amine-modified nanocellulose: an experimental and simulation study. Int J Environ Sci Technol 12(1):45–52. https://doi.org/10.1007/s13762-014-0659-z

Kaczmarek A, Cielecka-Piontek J, Garbacki P, Lewandowska K, Bednarski W, Barszcz B, Zalewski P, Kycler W, Oszczapowicz I, Jelińska A (2013) Radiation sterilization of anthracycline antibiotics in solid state. Sci World J 2013:258758. https://doi.org/10.1155/2013/258758

Kiraly R, Martin RB (1982) Metal ion binding to daunorubicin and quinizarin. Inorganica Chim Acta 67:13–18. https://doi.org/10.1016/S0020-1693(00)85033-1

Kooh MRR, Dahri MK, Lim LBL, Lim LH, Chan CM (2018) Separation of acid blue 25 from aqueous solution using water lettuce and agro-wastes by batch adsorption studies. Appl Water Sci 8(2):61. https://doi.org/10.1007/s13201-018-0714-x

Lafi R, ben Fradj A, Hafiane A, Hameed BH (2014) Coffee waste as potential adsorbent for the removal of basic dyes from aqueous solution. Korean J Chem Eng 31(12):2198–2206. https://doi.org/10.1007/s11814-014-0171-7

Lagergren SK (1898) About the theory of so-called adsorption of soluble substances. Sven Vetenskapsakad Handingarl 24:1–39

Langmuir I (1918) The adsorption of gases on plane surfaces of glass, mica and platinum. J Am Chem Soc 40(9):1361–1403. https://doi.org/10.1021/ja02242a004

Lian H, Meng Z (2017) Melt electrospinning of daunorubicin hydrochloride-loaded poly (ε-caprolactone) fibrous membrane for tumor therapy. Bioact Mater 2(2):96–100. https://doi.org/10.1016/j.bioactmat.2017.03.003

Lindberg RH, Namazkar S, Lage S, Östman M, Gojkovic Z, Funk C, Gentili FG, Tysklind M (2021) Fate of active pharmaceutical ingredients in a northern high-rate algal pond fed with municipal wastewater. Chemosphere 271:129763. https://doi.org/10.1016/j.chemosphere.2021.129763

Mahnik SN, Lenz K, Weissenbacher N, Mader RM, Fuerhacker M (2007) Fate of 5-fluorouracil, doxorubicin, epirubicin, and daunorubicin in hospital wastewater and their elimination by activated sludge and treatment in a membrane-bio-reactor system. Chemosphere 66(1):30–37. https://doi.org/10.1016/j.chemosphere.2006.05.051

Majumder A, Saidulu D, Gupta AK, Ghosal PS (2021) Predicting the trend and utility of different photocatalysts for degradation of pharmaceutically active compounds: a special emphasis on photocatalytic materials, modifications, and performance comparison. J Environ Manage 293:112858. https://doi.org/10.1016/j.jenvman.2021.112858

Mansour F, Al-Hindi M, Yahfoufi R, Ayoub GM, Ahmad MN (2018) The use of activated carbon for the removal of pharmaceuticals from aqueous solutions: a review. Rev Environ Sci Biotechnol 17(1):109–145. https://doi.org/10.1007/s11157-017-9456-8

Masanizan A, Lim CM, Kooh MRR, Mahadi AH, Thotagamuge R (2021) The removal of ruthenium-based complexes N3 dye from DSSC wastewater using copper impregnated KOH-activated bamboo charcoal. Water Air Soil Pollut 232(9):388. https://doi.org/10.1007/s11270-021-05333-7

Mello Souza D, Reichert JF, Ramos do Nascimento V, Figueiredo Martins A, (2022) Ozonation and UV photolysis for removing anticancer drug residues from hospital wastewater. J Environ Sci Health A Tox Hazard Subst Environ Eng 57(8):635–644. https://doi.org/10.1080/10934529.2022.2099195

Menazea AA, Eid MM, Ahmed MK (2020) Synthesis, characterization, and evaluation of antimicrobial activity of novel chitosan/tigecycline composite. Int J Biol Macromol 147:194–199. https://doi.org/10.1016/j.ijbiomac.2020.01.041

Mironova-Ulmane N, Kuzmin A, Steins I, Grabis J, Sildos I, Pärs M (2007) Raman scattering in nanosized nickel oxide NiO. J Phys Conf Ser 93(1):012039. https://doi.org/10.1088/1742-6596/93/1/012039

Nguyen VT, Vo TDH, Tran T, Nguyen TN, Le TNC, Bui XT, Bach LG (2021) Biochar derived from the spent coffee ground for ammonium adsorption from aqueous solution. Case Stud Therm Eng 4:100141. https://doi.org/10.1016/j.cscee.2021.100141

Osman AI, Fawzy S, Farghali M, El-Azazy M, Elgarahy AM, Fahim RA, Abdelmaksood MIA, Ajlan AA, Yousry M, Saleem Y, Rooney DW (2022) Biochar for agronomy, animal farming, anaerobic digestion, composting, water treatment, soil remediation, construction, energy storage, and carbon sequestration: a review. Environ Chem Lett 20(4):2385–2485. https://doi.org/10.1007/s10311-022-01424-x

Richardson Y, Blin J, Volle G, Motuzas J, Julbe A (2010) In situ generation of Ni metal nanoparticles as catalyst for H_2-rich syngas production from biomass gasification. Appl Catal A Gen 382(2):220–230. https://doi.org/10.1016/j.apcata.2010.04.047

Rivera-Utrilla J, Sánchez-Polo M, Ferro-García MÁ, Prados-Joya G, Ocampo-Pérez R (2013) Pharmaceuticals as emerging contaminants and their removal from water. A review. Chemosphere

93(7):1268–1287. https://doi.org/10.1016/j.chemosphere.2013.07.059
Sabitha M, Rajiv S (2015) Synthesis and characterization of biocompatible tigecycline imbibed electrospun poly ε-caprolactone urethane urea fibers. RSC Adv 5(3):2249–2257. https://doi.org/10.1039/C4RA08458F
Sajedi F, Moghaddas J (2022) Synthetic wastewater treatment of anticancer agents using synthesized hydrophilic silica aerogels. Sep Sci Technol 57(13):2041–2055. https://doi.org/10.1080/01496395.2022.2027446
Salunkhe P, Ma AV, Kekuda D (2020) Investigation on tailoring physical properties of nickel oxide thin films grown by dc magnetron sputtering. Mater Res Express 7(1):016427. https://doi.org/10.1088/2053-1591/ab69c5
Sen TK (2023) Adsorptive removal of dye (methylene blue) organic pollutant from water by pine tree leaf biomass adsorbent. Processes 11(7):1877
Sertoli L, Carnier R, Abreu CAd, Coscione AR, Melo LCA (2019) Coffee waste biochar: Charcterization and zinc adsorption from aqueous solution. Coffee Sci 14(4):518–529. http://www.coffeescience.ufla.br/index.php/Coffeescience/article/view/1634
Sharma AK, Desnavi S, Dixit C, Varshney U, Sharma A (2014) Extraction of nickel nanoparticles from electroplating waste and their application in production of bio-diesel from biowaste ICCCE2014, Singapore
Shin H, Tiwari D, Kim DJ (2020) Phosphate adsorption/desorption kinetics and P bioavailability of Mg-biochar from ground coffee waste. J Water Process Eng 37:101484. https://doi.org/10.1016/j.jwpe.2020.101484
Silva LSMS, Órfão JJM, Figueiredo JL (2001) Formation of two metal phases in the preparation of activated carbon-supported nickel catalysts. Appl Catal a: Gen 209(1):145–154. https://doi.org/10.1016/S0926-860X(00)00762-6
Sun Y, Xiong X, He M, Xu Z, Hou D, Zhang W, Ok YS, Rinklebe J, Wang L, Tsang DCW (2021) Roles of biochar-derived dissolved organic matter in soil amendment and environmental remediation: a critical review. Chem Eng J 424:130387. https://doi.org/10.1016/j.cej.2021.130387
Szafraniec E, Majzner K, Farhane Z, Byrne HJ, Lukawska M, Oszczapowicz I, Chlopicki S, Baranska M (2016) Spectroscopic studies of anthracyclines: Structural characterization and in vitro tracking. Spectrochim Acta A Mol Biomol Spectrosc 169:152–160. https://doi.org/10.1016/j.saa.2016.06.035
Tee WT, Loh NYL, Hiew BYZ, Hanson S, Thangalazhy-Gopakumar S, Gan S, Lee LY (2022) Effective remediation of lead(II) wastewater by Parkia speciosa pod biosorption: Box-Behnken design optimisation and adsorption performance evaluation. Biochem Eng J 187:108629. https://doi.org/10.1016/j.bej.2022.108629
Tejada-Tovar CN, Villabona-Ortíz A, Colpas-Castillo F, Sanmartín-Álvarez Z, Landázury-Galé D (2021) Cocoa husk-derived Biochars synthesized at low temperature impregnated with zinc chloride for removal of ibuprofen in different solutions. Ing Compet 24(1):e20510941. https://doi.org/10.25100/iyc.v24i1.10941
Temkin MI (1940) Kinetics of ammonia synthesis on promoted iron catalysts. Acta Physiochim URSS 12:327–356
Thotagamuge R, Kooh MRR, Mahadi AH, Lim CM, Abu M, Jan A, Hanipah AHA, Khiong YY, Shofry A (2021) Copper modified activated bamboo charcoal to enhance adsorption of heavy metals from industrial wastewater. Environ Nanotechnol Monit Manag 16:100562. https://doi.org/10.1016/j.enmm.2021.100562
Trivedi MK, Patil S, Shettigar H, Bairwa K, Jana S (2015) Spectroscopic characterization of chloramphenicol and tetracycline: An impact of biofield treatment. Pharm Anal Acta 6(7):395. https://hal.archives-ouvertes.fr/hal-01376485
Weber WJ, Morris JC (1963) Kinetics of adsorption on carbon from solution. J Sanit Eng Div 89:31–59
Wu FC, Tseng RL, Juang RS (2009) Characteristics of Elovich equation used for the analysis of adsorption kinetics in dye-chitosan systems. Chem Eng J 150(2):366–373. https://doi.org/10.1016/j.cej.2009.01.014
Zhong X, Zhang X, Zhou T, Lv G, Zhao Q (2022) Exploring kinetics, removal mechanism and possible transformation products of tigecycline by Chlorella pyrenoidosa. Sci Total Environ 817:152988. https://doi.org/10.1016/j.scitotenv.2022.152988